Simulated seasonal and interannual variability of mixed layer heat budget in the northern Indian Ocean

Clément de Boyer Montégut [1,4], Jérôme Vialard [1], S. S. C. Shenoi [2], D. Shankar [2], Fabien Durand [3], Christian Ethé [1], and Gurvan Madec [1]

Submitted to Journal of Climate, 30th April 2005
Accepted, 19th March 2006
(special issue on "Indian Ocean Climate System")

(1) Laboratoire d'Océanographie et du Climat: Expérimentations et Approches Numériques
Institut Pierre Simon Laplace
Unité Mixte de Recherche, CNRS/IRD/UPMC, Paris, France
(2) Physical Oceanography Division, National Institute of Oceanography
Dona Paula, Goa, India
(3) Laboratoire d'Etudes en Géophysique et Océanographie Spatiales
Institut de Recherche pour le Développement, Toulouse, France
(4) Now at Frontier Research Center for Global Change (JAMSTEC)
Yokohama, Japan

Corresponding author : Clément de Boyer Montégut, JAMSTEC Frontier Research Center for Global Change, 3173-25 Showa-machi Kanazawa-ku, Yokohama-city Kanagawa, 236-0001 JAPAN.
(clement@jamstec.go.jp)

Abstract

A global Ocean General Circulation Model (OGCM) is used to investigate the mixed layer heat budget of the Northern Indian Ocean (NIO). The model is validated against observations and shows a fairly good agreement with mixed layer depth data in the NIO. The NIO has been separated into three sub-basins: the western Arabian Sea (AS), the eastern AS, and the Bay of Bengal (BoB). This study reveals strong differences between the western and eastern AS heat budget, while the latter basin has similarities with the BoB. Interesting new results on seasonal timescales are shown. Penetration of solar heat flux needs to be taken into account for two reasons. First, an average of 28 W m^{-2} is lost beneath the mixed layer over the year. Second, the penetration of solar heat flux tends to reduce the effect of solar heat flux on the SST seasonal cycle in the AS because seasons of strongest flux are also seasons of thin mixed layer. This enhances the control of SST seasonal variability by latent heat flux. Impact of salinity on SST variability is demonstrated. Salinity stratification plays a clear role in maintaining a high winter SST in the BoB and eastern AS while not in the western AS. The presence of fresh water near the surface allows to store heat below the surface layer that can later be recovered by entrainment warming during winter cooling (with a winter contribution of +2.1°C in the BoB). On interannual timescale, the eastern AS and BoB are strongly controlled by the winds through the latent heat flux anomalies. In the western AS, vertical processes and also horizontal advection contribute significantly to SST interannual variability and the wind is not the only factor controlling the heat flux forcing.

1 Introduction

The Northern Indian Ocean (NIO), forced by the seasonally reversing monsoon winds, exhibits the two characteristics of the monsoon. First, it has a highly repetitive seasonal cycle: this implies a strong climatology. The monsoon winds reverse twice a year, blowing generally from southwest during the summer (June-September) and from the northeast during the winter (November-February) (Figure 1); March-May and October are the months of transition between the monsoons. Second, since no two monsoons are alike, in no two years does the NIO behave the same way: there is considerable interannual variability (Webster et al., 1998). This is reflected in the variations of temperature, salinity, and mixed layer processes, and in the heat and salt budgets. The interannual variability of the heat budget of the upper ocean (or mixed layer) is of paramount interest for air-sea coupling.

Several studies have examined the seasonal cycle of the mixed layer in the Arabian Sea (AS) (Shetye, 1986; Molinari et al., 1986; McCreary and Kundu, 1989; McCreary et al., 1993) and the heat budget of the upper ocean using data (Düing and Leetmaa, 1980; Rao et al., 1989; Rao and Sivakumar, 2000; Shenoi et al., 2002, hereinafter SSS02) and numerical models (Fischer, 2000; Prasad, 2004). Shenoi et al. (2005a) examined the heat budget of the near surface layers of the NIO using a model output and found that the model reproduces the surface heat content correctly, except during the spring warming (March-April), when the surface heat content is overestimated. Using diversified data sets, Düing and Leetmaa (1980) and SSS02 identified two mechanisms responsible for the summer cooling of the AS: western boundary upwelling and the export of heat through meridional overturning across the southern boundary of the AS. Such summer cooling is absent in the Bay of Bengal (BoB) owing to weak upwelling and meridional overturning owing to the weaker winds (Shenoi et al., 2005a).

The importance of salinity in the thermodynamics of the NIO, and its possible role in air-sea coupling, have aroused interest. Owing to the lack of salinity data on a scale comparable to temperature, especially sea surface temperature (SST), such studies have been restricted to the southeastern AS (Durand et al., 2004; Shenoi et al., 2004, 2005b; Shankar et al., 2004), the northern BoB (Vinayachandran et al., 2002), and a few other regions (Rao et al., 1985); they highlighted the importance of upper ocean stratification, caused by the fresh water fluxes, for the thermodynamics of the upper ocean. The stratification due to salinity leads to the existence of a barrier layer similar to that in the western tropical Pacific (see, for example, Vialard and Delecluse, 1998). Sengupta et al. (2002) highlighted the importance of penetrative solar radiation in determining the upper layer heat budget of the eastern AS. Both, the barrier layer, which often leads to subsurface inversions (Shankar et al., 2004; Durand et al., 2004), and the resulting penetrative solar radiation, play a crucial role in these regions.

The above studies were successful in describing the seasonal cycles, but the natural extension to interannual variability has not been made owing to the paucity of salinity data. It is this lacuna that numerical models can fill. Murtugudde and Busalacchi (1999,

hereinafter MB99) used an ocean general circulation model (OGCM) to show that the interannual variability of SST in the AS and in the Somali Current depends not only on variability in air-sea fluxes, but also on the wind forcing: in other words, oceanic processes play an important role in regulating SST. Vinayachandran (2004) used data from ARGO floats to show that length of the summer monsoon plays a key role in the summer cooling. None of the studies on interannual variability, however, are as comprehensive as those (cited above) on the seasonal cycle.

Hence, in this paper, we use an OGCM to investigate the interannual variability in the heat budget of the upper layers of the NIO. In doing so, we also include the effects of barrier layer and penetrative radiation. This investigation has several advantages over the previous studies mentioned above. The heat budgets of Düing and Leetmaa (1980) and Shenoi et al. (2002 and 2005a) estimated the budgets for fixed control volumes (50 m thick in the latter). Here, we estimate the heat budget of the mixed layer rather than the budget over a fixed layer because the mixed layer in the NIO (Figure 2) is often thinner than 50 m, implying that using a fixed control volume allows processes below the mixed layer to influence the SST. Following the suggestion of SSS02, we also estimate separately the heat budgets for the western and eastern AS; the 65°E meridian separates these two parts of the basin. The southern boundary of the regions of study, shown in Figure 1, is at 6°N. The heat budgets are computed online in the model using the time-varying MLD. The model computes air-sea fluxes internally, enabling a closed budget.

We begin by describing the model and the method used to estimate the budgets (Section 2); then we investigate the seasonal cycle (Section 3) and the interannual variability during 1993-2000 (Section 4). Section 5 summarises the paper.

2 Model and data

2.1 Physics of the model

The OGCM used in this study is the OPA model (Madec et al., 1999; see full documentation at http://www.lodyc.jussieu.fr/opa/), developped at the Laboratoire d'Océanographie DYnamique et de Climatologie (LODYC). OPA solves the primitive equations on an Arakawa C grid, with a second-order finite difference scheme. It assumes the Boussinesq and hydrostatic approximations, the incompressibility hypothesis and uses a free surface formulation (Roullet and Madec, 2000). The density is computed from potential temperature, salinity and pressure using the Jacket and McDougall (1995) equation of state. In its global configuration ORCA05, the horizontal mesh is based on a 0.5° by 0.5° Mercator grid, and following Murray (1996) two numerical inland poles have been introduced in order to remove the North Pole singularity from the computational domain. The departure from the Mercator grid starts at 20°N, and is constructed using a series of embedded ellipses using the semi-analytical method of Madec and Imbard (1996). Realistic bottom topography and coastlines are derived from the study of Smith

and Sandwell (1997), complemented by the ETOPO5 dataset. The maximum depth of 5000 m is spanned by 30 z-levels ranging from 10 m in thickness in the upper 120 m to 500 m at the bottom. The ocean model is run with a time step of 2400 s.

Lateral tracer mixing is done along isopycnals. Eddy-induced tracer advection is parameterized following Gent and McWilliams (1990) with coefficients decreased in the tropics between 20°N and 20°S. Momentum is mixed along horizontal surfaces using coefficients varying with latitude, longitude and depth. Vertical eddy diffusivity and viscosity coefficients are computed from a 1.5 level turbulent closure scheme based on a prognostic equation for the turbulent kinetic energy (Blanke and Delecluse, 1993). Double diffusive mixing (i.e. salt fingering and diffusive layering) is computed following Merryfield et al. (1999). A penetrative solar radiation corresponding to a type I water (Jerlov, 1968) is also used. The suitability of such a water type in the NIO will be discussed later in the paper.

2.2 Initialization and surface fluxes

The model run starts from an ocean at rest with January temperature and salinity fields of Levitus (1998) climatology. It is spun up for a 3-year period using a climatology of 1992-2000 forcing fields before starting the interannual simulation from 1992 to 2000. In the rest of the paper, we will study the 1993-2000 period.

The momentum surface boundary condition is given using the weekly ERS1-2 wind stress daily interpolated with a cubic spline method. The solar, longwave radiation and turbulent heat fluxes (and the evaporation) are computed from the semi-empirical or bulk formulae (Timmermann et al., 2005), which relate the fluxes to the SST (computed by the model) and to meteorological parameters (10 m wind speed, surface air temperature and relative humidity, cloudiness). The daily wind speed is given by interpolation of ERS1-2 weekly wind speed. The daily 2 m air temperature is extracted from the NCEP re-analysis (Kalnay et al., 1996). Monthly climatologies of relative humidity (Trenberth et al., 1989) and cloudiness (Berliand and Strokina, 1980) are used. We will discuss later in the paper the limitations inherent to using climatological values for relative humidity and cloudiness.

Fresh water fluxes from rain and river runoffs are important to maintain the Sea Surface Salinity (SSS) structure in the NIO, where important salinity gradients exist. Precipitation data come from the Climate Prediction Center Merged Analysis of Precipitation (CMAP) product (Xie and Arkin, 1996). This product has been shown to produce better surface salinity fields than others in the Indian Ocean (Yu and McCreary, 2004). Major river runoffs are also taken into account in our experiments, as they can have strong impacts on the Bay of Bengal upper structure (Han et al., 2001). The monthly values of river discharge (UNESCO, 1996) are introduced into the model by distributing the associated fresh water input as a precipitation on the points surrounding the mouth of the rivers. Figure 1 shows the location of the main river runoffs in the model.

A restoring term towards Levitus (1998) SSS is applied to the fresh water budget,

with a relaxation time scale of two months for a 50 m thick layer. While there is no physical justification for this feedback term as the atmosphere does not care about ocean surface salinity, it avoids SSS drift arising from the error in the prescribed fresh water budget. Simulating a proper SSS is indeed essential as it can have strong influences on the thermodynamic structure of the mixed layer (e.g., Vialard and Delecluse, 1998; Durand et al., 2004).

2.3 Mixed layer heat or salinity budget in the model

One of the main goals of this work is to understand how oceanic processes act to balance the atmospheric forcing and regulate the SST in the NIO. To do so, a mixed layer budget method (Vialard and Delecluse, 1998; Vialard et al., 2001) allows us to compute the vertically averaged temperature (salinity) tendency terms within the time-varying MLD. The depth of the mixed layer over which the diagnostic is applied, is computed using a density criterion. This depth is the bottom of the last model level from the surface, where density is smaller than the sea surface density plus 0.01 kg m^{-3}. Such a small criterion allows the vertically averaged mixed layer temperature T_{ml} to be a quite good proxy of the SST. Therefore the final equation for T_{ml} reads:

$$\begin{aligned}\partial_t T_{ml} \;=\; & \underbrace{-\frac{1}{h}\int_{-h}^{0} u\,\partial_x T\,dz - \frac{1}{h}\int_{-h}^{0} v\,\partial_y T\,dz}_{\text{horizontal advection}} \;\underbrace{-\frac{1}{h}\int_{-h}^{0} D_l(T)}_{\text{lateral processes}} \\ & \underbrace{-\frac{1}{h}\left(T_{ml}-T_{-h}\right)\left(w_{-h}+\partial_t h\right) - \frac{1}{h}\left[K_z \partial_z T\right]_{-h}}_{\text{subsurface vertical processes } (\simeq \text{ vertical mixing})} \;\underbrace{+\frac{Q_s\left(1-\mathcal{F}_{-h}\right)+Q_{ns}}{\rho_0 C_p h}}_{\text{atmospheric forcing } (F_T)} \quad (1)\end{aligned}$$

where h is the time-varying depth of model mixed layer; (u,v,w) are the components of ocean currents; $D_l()$ is the model lateral mixing operator (eddy-induced tracer advection will be grouped in the lateral processes term as a parameterization of the subgrid scale lateral mixing); T_{-h} is the temperature at the base of the mixed layer; K_z is the vertical mixing coefficient for tracers; Q_{ns} and Q_s are respectively the nonsolar and solar components of the total heat flux; $\mathcal{F}_{-h}$ is the fraction of solar shortwave radiation that penetrates through the base of the mixed layer; ρ_0 is the seawater reference density; and C_p is the seawater heat capacity. This equation clearly shows the importance of the MLD in the tendency balance (1) and hence in the diagnostic of the mixed layer temperature. We have the same equation for the salinity budget by replacing temperature T and T_{ml} respectively by salinity S and S_{ml} and taking as the forcing term the following expression: $F_S = \frac{1}{h}\,SSS\;(E-P-R)$, with SSS the sea surface salinity, and E, P, R, respectively the evaporation and precipitation fluxes and the river runoff.

In equation (1), the subsurface vertical processes term represents the heating rate due to all oceanic vertical processes occuring at the base of the mixed layer. These are vertical

advection ($-\frac{1}{h}w_{-h}\left(T_{ml}-T_{-h}\right)$), entrainment mixing ($-\frac{1}{h}\partial_t h\left(T_{ml}-T_{-h}\right)$), and vertical turbulent mixing ($-\frac{1}{h}\left[K_z\partial_z T\right]_{-h}$). Following Vialard et al. (2001), those terms have been grouped together due to the lagrangian nature of our diagnostics.

It is also important to note that horizontal advection (and lateral processes) term not only represents an exchange within the mixed layer. It also represents an exchange between the mixed layer and the interior ocean in regions of high mixed layer depth gradient. Therfore, in doing integrated budgets over the AS or the BB, the horizontal advection term is not only what enters/exits at the boundary of the domain but also what enters/exits at the mixed layer bottom.

3 Seasonal variability

3.1 Validation of the model

The time-varying depth of the mixed layer is a crucial parameter for the mixed layer heat budget and hence the SST (e.g., Chen et al., 1994; Qiu et al., 2004). Modelling properly the mixed layer physics and diagnosing a correct MLD is the first necessary step to assess the surface temperature or salinity budgets.

The model MLD has been compared to a gridded MLD product, resulting from interpolation of MLD estimated on more than 4 million individual profiles and gridded on a 2° resolution grid (de Boyer Montégut et al., 2004). This product has recently been upgraded to include ARGO floats which considerably improves the coverage in the Indian ocean, and to include estimates of the barrier layer thickness (de Boyer Montégut et al., 2004; Mignot et al., 2006). Figure 2 shows the seasonal MLD from the model and from observations. The method to compute the MLD is the same for both sources, being based on the average of MLDs from instantaneous profiles. The model online heat budget computation were performed with a 0.01 kg m^{-3} criterion for the MLD. Because of the diurnal variability, a higher criterion (0.03 kg m^{-3}) has to be taken in the data (de Boyer Montégut et al., 2004). Nevertheless it has been checked that the MLD obtained from the model with both criteria is almost identical (about 5 m maximum difference on annual mean state over most of the region, not shown).

Seasonal MLDs from the model are in good agreement with observations, and the main features are well reproduced. For example, the AS exhibits a MLD with a large semi-annual cycle which is characteristic of that region in both data and model. It is the consequence of the annual cycle in the surface forcing due to seasonnally reversing monsoon winds (Schott and McCreary, 2001).

The summer and winter monsoon MLDs in Arabian Sea are on average about 10 m deeper in the model than in the observations. However these differences are regionally dependent. The model is systematically deeper than observations in regions of negative Ekman pumping. For example during the summer monsoon, a deep bias is found in the model southeast of the Findlater (1969) Jet axis (Figure 2). The model therefore seems

to enhance the effect of negative Ekman pumping on MLD deepening. Previous studies actually showed that Ekman pumping does not dominate the upper-ocean response in the AS but rather acts as a modulation of wind-driven entrainment in summer, and convective overturning in winter (e.g., Lee et al., 2000; Fischer et al., 2002). In addition, McCreary et al. (2001) also noted the same deep bias for their model in winter AS and suggested that it could result from deficiencies in the parameterization of their mixed layer physics based on a diagnostic production of turbulent kinetic energy.

In summer and fall, shallow MLDs are found in the model along the coast of India. This shallow MLD in the model is fairly realistic and is likely linked to the advection of the low salinity water along the coast by the East India Coastal Current after the summer monsoon runoffs in the north of the Bay (Eigenheer and Quadfasel, 2000). That feature is not found in the observed MLD but this might be due to poor observational coverage close to the coast of India. The MLD climatology based on temperature only data has a much better coverage. It does present shallow MLDs along the coast (de Boyer Montégut et al., 2004) and the model MLD is indeed in good agreement with the climatology in that area.

A region of particular interest is the southeastern Arabian Sea. Recent papers have shown that thin mixed layer (less than 20 m) and thick barrier layer occuring in winter have potential impact on SST maximum and onset of summer monsoon (e.g., Durand et al., 2004; Masson et al., 2005). Such a feature is present in both data and model, and barrier layer thickness is also in good agreement between data and model with maximum values over 20 m in February (not shown).

Other validations (not shown) to observed seasonal cycle of SST (Reynolds and Smith, 1994), gridded sea level (produced by CLS and available at http://www.jason.oceanobs.com/), and sea surface salinity (Levitus, 1998) were performed. The SST seasonal cycle is very well reproduced (with correlations above 0.8 almost everywhere). The sea level seasonal cycle is in good agreement in regions where it is dominated by the large scale circulation and slightly underestimated in regions of strong eddy activity. The large scale surface currents seasonal cycle is in good agreements with the description made by Schott and McCreary (2001). The overall seasonal upper ocean variability in the NIO is hence reasonably reproduced by the model. We can thus use the model to investigate the seasonal heat budget in the NIO.

3.2 The mixed layer heat budget

In this section, the model is used to evaluate the seasonal heat budget of the mixed layer in the NIO. The previous most comprehensive study of this type, using observations, was the one from SSS02. In addition of using a model, the present study has a few differences with SSS02. First, we integrate the heat budget over a time varying mixed layer, rather than a fixed 50 m layer. Second, as suggested by SSS02 we chose to present separatly the budget for eastern and western AS, delimited by the 65°N meridian to illustrate the different behaviour of the western AS (where upwelling processes play an

important role) and eastern AS. Third, we take the solar energy penetration into account in this study: with the shallow mixed layer that sometimes occur in this region, this can indeed result in a significant part of the incoming solar heat flux penetrating below the mixed layer and heating deeper layers. In the overview below, we will brush the main features of the three sub-basins and underline the new results in this study, compared to SSS02 or MB99. We will then describe the seasonal heat budget in the three sub-basins in more detail.

3.2.1 Overview

The mean temperature over 0-50 m (T50) has been indicated on Figure 3, since SSS02 computed the heat budget over this fixed layer. It can be seen that there are important differences that appear seasonally between T50 and mixed layer temperature. For example, a difference of more than 1 °C can be observed in the western AS in May when mixed layer is at its shallowest. This shows that a precise quantification of the processes that affect SST require an integration over the time-varying mixed layer depth. SST is not shown on Figure 3 as it is very similar to the mixed layer temperature, which means that the latter is a quite good proxy of SST.

The observed and modeled MLDs are plotted on Figure 3 as MLD is an essential parameter in these budgets. The basin scale agreement is fairly good except during winter monsoon in western AS. The same comparison between data and model is done for barrier layer thickness. No barrier layer occurs in the western AS. In the eastern AS and in the BoB, barrier layer thickness is maximum in winter in both data and model.

The surface heat fluxes have globally the same behaviour in the three basins (Figure 3). The semi-annual cycle of the net heat flux is essentially driven by latent heat flux variations, with the solar heat flux playing a secondary role. Long wave radiation is not negligeable ranging between 30 and 80 W m^{-2} but has a small variability, while the sensible heat flux is nearly nul at any time. Table 1 shows the annual net heat flux for the three sub-basins. It makes an annual net heat gain of 28.3 W m^{-2} for the AS, which is in good agreement with the 24 W m^{-2} of Düing and Leetmaa (1980). However, when comparing our fluxes with the recent Southampton Oceanographic Center (SOC) climatology (see SSS02, their figure 8), one realizes that we have a weaker shortwave gain in all basins and a stronger latent heat loss in the AS during monsoons. That is also the case for older climatologies and for NCEP or ECMWF heat fluxes (Weller et al., 1998). These fluxes differences are addressed further in section 5.

Taking the penetrative solar heat flux (Q_{pen} on Figure 3) into account is important, especially in regions of thin mixed layer (Lewis et al., 1990; Anderson et al., 1996). It is the case in the western Arabian Sea where up to 65 W m^{-2} can be lost beneath the mixed layer in April when it reaches a minimum of 15 m. This represents roughly half of the net heat flux into the ocean and neglect of Q_{pen} would increase the predicted SST by 3.5°C over the month of April. Table 1 shows the effective net heat flux into the surface mixed layer (Q_{eff}). In our case it turns the annual net heat gain at the surface in annual

net heat loss for the mixed layer in the eastern AS and the BoB. The penetration of solar heat flux also contributes to damp significantly the solar heat flux variability in the mixed layer (Table 1). Inter monsoon seasons indeed correspond to maximum net surface heat flux and minimum mixed layer depth which results in a compensating effect for the net heat flux received by the mixed layer. In the AS, this reduces the variability of the solar heat flux by roughly 40 percent. In the BoB where the MLD is very shallow, reaching maxima of only 35 m, heat loss under the mixed layer occurs all year long (Figure 3c).

Influence of the salinity on the mixed layer heat budget appears to be an important factor to understand why the winter SST decrease is more important in the western than in the eastern AS (Figure 3). Both sub-basins experiences an atmospheric heat loss of 2.3°C during winter (November through January). However, heat accumulated in the barrier layer in the eastern AS warms the surface layer by 0.4°C (Table 2). Meanwhile, no barrier layer developps in the western AS and vertical mixing cools the mixed layer by -0.8°C. This can contribute to the winter SST difference between the two sub-basins. As will be seen in the following subsection, the BoB also experiences a moderate heat loss during winter in spite of high atmospheric heat loss. This is due to the warming effect of the heat accumulated in the barrier layer in the previous seasons. Now that we have brushed the common features to the three basins and emphasize some new results, let us investigate in more detail the particularities of each basin. As processes are most often linked together, we will now stick to a description of the heat budget season by season.

3.2.2 Western Arabian Sea

The western AS SST experiences two seasons of warming during intermonsoons (March-April-May and September-October), and two seasons of cooling during both monsoons (June-July-August and November through February). During intermonsoon seasons, atmospheric forcing and subsurface vertical processes are the driving mechanisms of the SST variability. In winter, the evolution of SST is driven by atmospheric forcing alone. On the other hand, in summer all oceanic processes act to balance the SST tendency (Figure 3a, middle panel). The summer heat budget in this region is strongly dominated by the upwellings along Somali and Oman coasts as will be seen later in this section. During this season, one can notice that the two curves corresponding respectively to atmospheric forcing (F_T in equation (1)) and to Q_{eff} can be quite different (Figure 3a). This is due to the non linearity of the spatial averaging over the basin : $\overline{Q_{eff}} = \overline{\rho_0 C_p F_T h} = \rho_0 C_p \left(\overline{F_T}\,\overline{h} + \overline{F_T{}'h'} \right)$. In addition, during summer F_T and h are strongly correlated spatially so that the non linear term is not negligible (h is small and F_T is high in coastal zone, and vice versa elsewhere). We will therefore make a separate heat budget for coastal and non coastal zone to show the differences between those two regions during summer (Figure 4).

Spring is the first warming phase, with atmospheric forcing tendency increasing to its maximum in April. Very low winds result in reduced heat losses. This is combined

with a very shallow mixed layer ($\simeq$ 15 m) which is also an essential factor for increasing the atmospheric heating rate. SST becomes homogeneous and very high all over the AS. Consequently vertical temperature gradient with subsurface temperature increases and the cooling effect is more marked. Beginning of upwellings in May also increases the subsurface vertical processes cooling. Solar heat flux is maximum due to clear sky conditions and penetrative solar radiation is also maximum during this period due to the thin mixed layer ($\simeq$ 50 W m^{-2}). This contributes to reduce the surface layer heating and to heat up the subsurface water underneath the mixed layer.

With the summer monsoon onset, oceanic processes become a strong contribution in the heat budget and contribute to counterbalance the heat accumulated in the previous months near the surface. As shown in other previous studies (e.g., McCreary and Kundu, 1989; SSS02), cooling by subsurface vertical processes is very important in western AS in summer. During that season, mixed layer heat budget can be separated between coastal zone (about 350 km wide, Figure 1) and central western AS (Figure 4). Western AS heat budget features observed on Figure 3a (middle panel) are therefore mainly dominated by strong oceanic processes occuring in the coastal upwelling areas (Figure 4a). On the other hand, the central western AS closely resembles the eastern AS, without any influence of barrier layer warming in winter (Figure 4b). In the upwelling regions, vertical advection maintains a shallow MLD (Figure 2a) and also enhances the stratification below the mixed layer. The 20 °C isotherm lies at 40 m near the Oman coasts while reaching 160 m in the center of the basin (not shown). Vertical mixing between the mixed layer and the cold upwelled water that lies below creates the greatest part of the cooling in the western AS coastal zone (Figure 4a). In central western AS, both vertical processes and horizontal advection contribute to cool the SST (Figure 4b). Following the eastward summer monsoon current across the Arabian Sea (Shankar et al., 2002), cold water from the Oman and Somali upwelling regions is advected eastward towards the interior basin. It contributes to a -0.85°C cooling integrated during summer months. This is lower than what is found by MB99 in their Figure 7a for horizontal advection in a central AS basin (equivalent to about -1.2°C cooling over summer). As upwelled surface waters are cold, latent heat losses are reduced and can even reach zero near the coast. This results in high atmospheric heating rate in upwelling areas, that partly balances subsurface cooling (Figure 4a). Lateral processes also play a role in heating the mixed layer during summer monsoon (Figure 4a). The latter are dominated by Gent and McWilliams (1990) eddy-induced advection localised in the dynamically unstable upwelling areas of Oman and Somali (not shown). One can also note that, depsite MLD is approching 50 m depth on average over western AS in summer, T[ml] is quite different from T50. This is due to upwelling areas where the thermocline (20°C isotherm) can reach shallow depths of 40 m with a very rapid decrease of temperature underneath the mixed layer.

During fall intermonsoon (September-October), the mixed layer shoals and warms up due to reduced winds and latent heat losses. It is however counterbalanced by subsurface vertical processes cooling in the upwelling regions. Upwellings have indeed weakened but the stratification at the base of the mixed layer is still well marked with a sharp and

shallow thermocline in such areas. This results in a still significant cooling due to vertical mixing in those areas.

In winter (November through February) the cooling of SST in the western AS is driven by atmospheric forcing which contribute to a -2.3°C cooling. The heat losses are due to two combined factors. The sustained winds of the northeast monsoon are cold and dry, and lead to a strong evaporative cooling. This is combined to reduced insolation in winter, especially in the northern part of the basin. The mild sustained wind induces a mixed layer deepening mostly through a negative buoyancy flux at the air-sea interface (Lee et al., 2000). Rochford et al. (2000) noted a heating contribution from northward horizontal advection of warm water in the south of the western AS. Our estimation in this area is in acceptable agreement with theirs but it is rather weak compared to atmospheric forcing on the basin scale (0.6°C warming over the season).

3.2.3 Eastern Arabian Sea

As in the western part of the AS, two warming phases occur during intermonsoons, and two cooling phases during both monsoons. However oceanic processes are very weak and the SST tendency is mainly driven by atmospheric forcing all over the year (Figure 3b, middle panel).

In spring, a strong atmospheric heating occurs and vertical mixing is cooling the basin as in the western AS but to a smaller extent. At the end of spring, a continuous stratification has formed in the upper 50 m (from about 28.5°C at 50 m to nearly 30°C at sea surface), due to weak winds and strong penetrative solar heating (Sengupta et al., 2002). In summer, net heat flux becomes markedly negative while it remains near zero in the west. Latent heat flux is stronger because eastern AS stays warmer, above 28°C until mid-August, which allows deep convection to occur. Latent heat flux is the main contributor to cooling during summer, while horizontal advection of cold water from the west remain very weak ($\simeq$ -0.1°C cooling). The cooling contribution to subsurface vertical processes is also much smaller than in the west (only about 0.6°C cooling), because the subsurface water may have been heated in the previous season by the penetrative solar heating. As noted by Shetye (1986), a part of this accumulated heat may also be transported vertically through downwelling to deeper layers. The absence of cooling oceanic processes in this basin in summer contribute to maintain a high SST during that period.

Fall intermonsoon in the east is analogous to what happens in the west, except that nearly no oceanic processes act to counterbalance the atmospheric heating. Winter heat fluxes act to cool down SST and deepen the mixed layer through a negative buoyancy flux at the air-sea interface as in the western AS. Meanwhile, a barrier layer has developped in eastern AS (Durand et al., this issue), as seen on Figure 3b, upper panel. The heat accumulated in the barrier layer contribute to warm the deepening mixed layer through subsurface vertical processes during winter (Figure 5). On the basin scale it represents a total 0.4 °C heating throughout winter. This heating by subsurface vertical processes can explain the higher winter SST in eastern AS than in the west (Table 2).

3.2.4 Bay of Bengal

In the BoB, SST evolution is rather weak during summer and fall while in winter and spring, SST changes are comparable to those in the AS (Figure 3c).

In spring, net heat flux warms up the surface layer as in the Arabian Sea. The resulting temperature stratification at the surface provocates the annihilation of the precedently formed barrier layer. A contribution of subsurface cooling occurs as in Arabian Sea. Penetrative solar radiation also reaches its maximum ($\simeq$ 45 W m^{-2}) and heats up subsurface water creating a continuous vertical stratification in the upper 50 m.

In summer, the BoB experiences lower heat loss due to lower atmospheric forcing than in the eastern AS. Solar heat flux is smaller because of high cloud cover (about 80 percent in August) but latent heat flux is also weaker due to lower winds over the bay. Subsurface vertical processes tendency is negative on the basin scale due to the weak upwelling along east coast of India (Shetye et al., 1991; Shenoi et al., 2002), and to the Sri Lanka cold dome (Vinayachandran and Yamagata, 1998). Contribution of the vertical processes is however only a -1.0°C cooling from May to August, which is negligible compared to the one in the western AS. This differs from results of SSS02 or MB99. SSS02 found an important contribution of vertical processes (diffusion of heat through the bottom) in the BoB. However this may be due to the fact that they compute this term on a 50 m depth layer whereas the MLD in the BoB is always less than 35 m with a growing barrier layer beneath it. Another reason for the difference may be because SSS02 used a constant vertical diffusion coefficient. MB99 also pointed out marked entrainment cooling in the BoB in June and July. They noticed that it should be viewed with caution since they do not include some river discharges which can be responsible for barrier layer formation and surface warming.

In fall, SST hardly warms up. Solar heat flux is weak compared to eastern AS due to high cloud cover over the bay. Barrier layer continues to build up while fresh water from precipitation and runoff is advected in the bay along the east coast of India. It reaches a maximum value around 20 m on average in winter. During winter, relatively high cloud cover combined with northeasterly cold dry winds result in a strong heat loss due to surface fluxes over the bay (-4.9°C cooling in winter). Mixed layer deepens to its maximum entraining warm subsurface water of the barrier layer (Figure 5). This water has been heated in the preceding spring season through penetrative solar heating. This mechanism could establish a potential link between winter SST and SST in the previous spring season. The quasi-biennial variability of the summer monsoon seems to be influenced by Indian Ocean SST in the previous winter and spring seasons (Li et al., 2001), so penetrative solar heat flux may play a role in such a variability. The contribution of subsurface warming reaches 2.1°C over winter season (Table 2). This is a key process that inhibits the Bay to loose heat during winter and keeps its winter SST higher than in the western AS despite strong atmospheric cooling.

Results of the seasonal mixed layer heat budget are qualitatively in agreement with previous studies, especially the one by SSS02, although there are quantitative differences

due to the fact that SSS02 compute their budget on a fixed 50 m layer. Mixed layer salinity budget was also investigated in the three basins and is consistent with previous studies (e.g., Rao and Sivakumar, 2003). Horizontal advection play a dominant role to freshen the western AS evaporation basin during both monsoons and to drive the variability of SSS in the eastern AS (not shown). Additionnaly, some new important results have been found. First, the separation between eastern AS and western AS shows that the two latter are strongly different. The eastern AS basin can be considered as a transition between western AS and BoB. That basin experiences strong summer monsoon winds as in the western AS but no oceanic processes act to cool the SST in summer. It also experiences high summer precipitation and the salinity effect which maintains its winter SST high as in the BoB. Second, penetration of solar heat flux is a key feature of the forcing. It causes an average of 28 W m^{-2} to be lost beneath the mixed layer over the year, turning the atmospheric contribution of the eastern AS and BoB to a negative one (in our case). Furthermore it tends to reduce the amplitude of the warm phase of the SST seasonal cycle in the AS because seasons of strongest positive flux are also seasons of thinest mixed layer. Another striking result is the important role of salinity in the seasonal heat budget of the NIO. Salinity effects can explain why winter cooling is greater in the western than in the eastern AS (Table 2). Heat accumulated in the barrier layer in the eastern AS warms up the mixed layer in winter by 0.4°C while the western AS experiences a subsurface heat loss of -0.8°C. SSS02 showed why the BoB remains warmer than the AS during summer. Salinity effects contribute to enhance that SST difference in winter. The BoB experiences a high barrier layer warming effect of 2.1°C in winter (Table 2) which counterbalances the great atmospheric cooling (-4.9°C) and enables the Bay winter temperature to stay above 27°C.

4 Interannual variability of SST

At interannual timescales subsurface variability is not well sampled by observations. Models offer a good alternative to investigate the regulating mechanisms of SST in the NIO at those timescales. Furthermore, the good agreement between the results of the previous section and other studies (e.g., SSS02; Rao and Sivakumar, 2003) gives some confidence in the model. In this section, after an overview of the interannual variability during the 1993-2000 period, we will investigate the heat budget in the model in more detail in our three regions of interest.

4.1 Overview of the 1993-2000 period

Figure 6 shows the interannual anomaly of SST in the three regions, after filtering the intraseasonal variability. Note that there is also a strong intraseasonal variability of the SST and heat budgets at the basin scale, as noted in previous studies (e.g., Vecchi and Harrison, 2002) but we will not investigate it here. The main climate anomalies

reported elsewhere in literature in the Indian ocean for this period are the 1994 Indian Ocean Dipole (IOD) (Behera et al., 1999), a longer than usual monsoon in 1996 (Halpert and Bell, 1997), the impacts of the 1997-98 El Niño and of the 1997 IOD (Webster et al., 1999).

IOD events generally induce weak positive anomalies in the AS between July and October (Saji et al., 1999). Despite this, the 1994 event is rather associated to cool anomalies peaking in the middle of the year. These anomalies are rather weak, however (less than 0.5°C), and not especially remarkable when compared, e.g., to the cold anomaly in 1999.

The end of 1996 is marked by a clear cooling in the AS (with cold anomalies up to 0.7°C). Vinayachandran (2004) pointed out that a long summer monsoon can be a decisive parameter for summer cooling in the AS, as it is observed in Reynolds SST but not as much in the model (Figure 6). We can also note that enhanced deep convection appeared over the AS during June, with an over 10 percent increase in NCEP cloud cover over most of the western AS (Lander et al., 1999).

The cold anomaly was then followed by a clear warming of the three sub-basins from mid 1997 to early 1999 with anomalies above 0.5°C lasting several months. This period was associated to an El Niño in the tropical Pacific, which is known to be associated to a basin-scale warming in the Indian Ocean (Yu and Rienecker, 2000). The IOD that happened in 1997 probably also contributes to the persistent warm anomalies in the NIO (Saji et al., 1999). The warm anomalies are followed by cold anomalies peaking in the middle of 1999 in the three basins. There were no clear anomalies in the BoB in 2000, and the anomalies in the AS were quite similar to those of the previous year, with about 0.5°C cold anomalies peaking during the beginning of summer monsoon.

Figures 7 to 9 show various quantities averaged over the three sub-basins, including the interannual anomalies of the heat budget. Before we go into the details of each sub-basin in the following section, we will describe here some features common to the three sub basins. Panel (a) shows the interannual anomalies of the mixed layer depth and of the wind. It is worth noting that the wind strongly controls the mixed layer depth over the three sub-basins. Stronger wind will indeed enhance vertical mixing both by creating shear at the mixed layer bottom, but also by enhancing evaporative cooling and diminishing the vertical stability of the water column. Panel (c) of the three figures shows the interannual anomalies of the net and latent heat flux for the three sub-basins. The net heat flux interannual variability is dominated by latent heat flux, with other contributions from solar, longwave and sensible heat flux playing a negligible role. Two other curves show the latent heat flux recomputed from the Reynolds and Smith (1994) SST rather than the model SST (we explain below the interest of this computation), taking into account or neglecting the air-sea humidity gradient interannual anomalies in the computation (but always taking into account wind interannual anomalies). The two curves are very close most of the time over the three sub-basins, suggesting that wind interannual variability is the main factor that drives the latent heat fluxes (and thus net heat fluxes) interannual variability. Some local studies in the AS (Konda et al., 2002; Vecchi et al., 2004) suggest that anomalies of air temperature and humidity sometimes can play a significant role in

the latent heat flux, and this is indeed sometimes punctually the case (e.g. in the WAS in late spring 2000). But overall, at the basin scale, the latent heat flux anomalies are mainly driven by wind speed anomalies as it is usually the case in tropical regions (Cayan, 1992).

Figure 6 shows that the model reproduces generally fairly well the SST variability over the three sub-basins, with however sometimes significant departures from observations. For example, in 1996, the model underestimates the cold anomaly in the western AS, and also has a warm bias in the BoB. Since the heat fluxes are computed with bulk-formulae using the model SST, this will affect the surface fluxes. To validate the surface fluxes computed by the model, we have also recomputed the surface fluxes using Reynolds and Smith (1994) SST. This provide some validation of the model interannual flux anomalies. In most occasions, since the model SST is close to observations, the fluxes computed from the model are consistent with those from observations. But in some cases, as in 1996, there can be important differences: the model latent heat flux anomaly is negative while the one computed from observations is positive (Figure 7). In 1996, the model is warmer than observations and thus warmer than the prescribed air temperature (which is always close to the SST). This difference grows to large values creating an unrealistic SST-air temperature gradient. This gradient becomes strong enough to exert a stronger control over the latent heat flux anomaly than the wind. The difference between the model latent heat flux and the one computed from Reynolds can be compared to the relaxation term used in many other ocean modelling studies. When this terms becomes large, it simply means that missing processes in the model simulation (e.g. in our case, the absence of interannual variability of the clouds and relative humidity or deficiencies in the simulated upwelling) is compensated for by a flux anomaly. In the following subsections, we will thus remain careful in attributing the SST variability to a specific process during periods when this "hidden relaxation term" is strong.

4.2 Western Arabian Sea

Figure 7 (middle panel) shows the various terms of the heat budget for the western AS. Atmospheric forcing and vertical processes contribute significantly and alternatively drive the total tendency. Vertical subsurface processes can contribute as a negative feedback to the total tendency (e.g. during the 1996 cooling, or in 1999), but can drive the total tendency in some occasion (1993, 1995, 1998). Horizontal advection is weaker than vertical processes, but cannot be neglected. It generally acts as a negative feedback to the atmospheric forcing (e.g. advection warms during the 1996 cooling and cools during the 1997 warming). Lateral processes are dominated by Gent and McWilliams (1990) advection and it is negatively correlated to subsurface vertical processes since its effect is to counteract the enhancement of the frontal areas in upwelling. The atmospheric forcing tendency depends both on the net heat flux interannual variations and on the depth of the mixed layer (equation 1). It can be seen on Figure 7 that the interannual variations of this term are largely driven by the latent heat flux. However, when comparing 1998-1999 winter (high MLD conditions) and 1999 fall (low MLD conditions), we can see that mixed

layer depth seasonal variability modulates this term at the second order.

As noted previously, the 1996 cooling phase may correspond to the effect of a hidden relaxation term acting to compensate for missing cooling processes in our model, such as the influence of an increased cloud cover (a climatological cloud cover is used). The model seems to fail in reproducing the cooling effect of a longer than usual summer monsoon. During that cooling phase, vertical mixing tendency anomaly is positive which is consitent with a weaker upwelling due to weaker winds. Horizontal advection is usually associated with an influx of cold water through the sloping mixed layer around the upwelling region. The weaker upwelling also leads to a positive tendency anomaly of horizontal advection.

The following warming period, from December 1996 to May 1998 is characterised by generally negative anomalies of the winds, except in december 1997. During this period latent heat flux is rather driven by these winds anomalies which lead to the warming phase. Vertical processes are again rather well correlated with wind (reduced wind in 1997 lead to reduced cooling by vertical processes). Horizontal advection is here associated to a significant cooling during summer, that resists the general warming tendency.

In summer 1998, a cooling phase begins until the next summer monsoon. The 1998 summer monsoon experiences positive winds anomaly and therefore an increased heat loss from atmospheric forcing and vertical processes. Because of strong horizontal gradients of temperature around the enhanced upwelling, lateral processes warm the mixed layer at a higher rate than usual. The intense cooling then resumes in spring 1999, largely driven by strong winds and increased evaporative cooling.

The end of 1999 is a good example of summer monsoon for which atmospheric forcing and vertical processes are acting against each other as in 1996. The reasons are mainly the same. As SST has been considerably cooled during pre monsoon, latent heat flux anomaly in summer is partly driven by humidity at the sea surface which is anomalously low (because of a low temperature) and result in a positive anomaly of the flux tendency. Subsurface processes and horizontal advection are enhanced due to rather stronger winds. As in MB99, we find that vertical oceanic processes have an important contribution to SST anomalies in the western AS. Additionnally, the mixed layer heat budget showed us that regulation of SST interannual anomaly in that area appears to be quite complicated, without any simple relation between the different tendency terms and the total tendency of SST.

4.3 Eastern Arabian Sea

In the eastern AS, the interannual temperature anomaly is primarily driven by atmospheric forcing (Figure 8). MB99 found that variability in SST interannual anomaly in the AS or BoB depends on both surface heat fluxes and wind forcing. Here, it is shown that vertical mixing actually plays a secondary role and generally contributes as a weak negative feedback. Oceanic processes thus play a lesser role than in the west, where more marked dynamical structures exist.

The wind variability exerts a strong control in this basin and may explain a large part of the SST interannual variability. Net heat flux anomaly are almost entirely driven by latent heat flux anomalies (lower pannel on Figure 8). These latent heat flux anomalies are themselves quite correlated to wind anomalies (upper and lower pannel). Strong winds (as, e.g., in late 1996) generallly lead to stronger evaporative cooling and to a negative tendency of the forcing term. The wind also exerts a strong control over the mixed layer (upper pannel) with strong wind deepening the mixed layer. In conditions of thin mixed layer as in pre- and post-monsoon season, the effect of layer variations are pre-dominant in the variations of vertical term (see equation 1). A deeper mixed layer (and enhanced mixed layer heat capacity) lead to a weaker cooling (i.e. a positive interannual anomaly, for example in fall 1998). This explains the weak negative feedback due to vertical processes.

However, in winter 1997/1998, the strong evaporative cooling is not driven by the wind (which is near normal) but rather by the higher than usual SST leading to an increased latent heat flux. Additionnaly, the interannual anomalies of the vertical processes are not always due to mixed layer heat capacity variations. In winter 1998 the positive anomaly of vertical processes is linked to a positive anomaly of the barrier layer thickness which may be the source of heat for the mixed layer at that time.

4.4 Bay of Bengal

In the BoB, the total tendency anomaly is mainly driven by atmospheric forcing (Figure 9). As in the eastern AS, vertical mixing acts as a negative feedback. The wind is the essential driving factor of the interannual variability in the BoB. The latent heat flux interannual anomalies (that dominate the net heat flux anomalies) are largely driven by wind variability (even if other factors sometimes play a role). The resulting net heat flux variations drive the SST warming or cooling over most of the basin. Other terms can sometimes play a significant role (and even revert the tendency like in early 1998), but the only one having a systematic phase relation with forcing is the vertical processes. The negative feedback from the vertical processes is more difficult to explain here than in the eastern AS, because of the reversing sign of the vertical processes during the seasonal cycle (vertical processes warm the surface in october-january because of barrier layer). However it seems that interannual barrier layer variations do have an impact on the vertical processes, with thicker barrier layers leading to a positive anomaly.

5 Summary and discussion

In this paper, a global OGCM simulation of the 1993-2000 period is used to study the mixed layer heat budget of the NIO. Validations of the model mixed layer depth, sea surface temperature, sea level and surface currents show a qualitative agreement between the model and available observations. The NIO can be separated into three sub-basins. In

the BoB and eastern AS (with a meridional separation at 65°E), the SST seasonal cycle is very similar, and is essentially driven by atmospheric heat fluxes, with oceanic processes playing a secondary role. In the western AS, surface forcing is still the dominant process but with a large contribution from oceanic processes, especially during the summer monsoon (vertical processes in the upwelling region and horizontal advection through the sloping mixed layer). In the three sub-basins, however, the wind is a primary factor in driving the SST seasonal cycle. Net heat flux seasonal cycle is indeed largely controlled by latent heat flux variations, since the solar flux effect is damped by the effects of light penetration (incoming solar heat flux is weaker during the monsoon because of clouds, but the deeper mixed layer captures a larger fraction of the incoming flux). Penetrative solar heat flux indeed represents an average of 28 W m^{-2} heat loss beneath the mixed layer over the year, with a part of it that might be advected to deeper layers. This can turn the atmospheric contribution of the eastern AS and the BoB into a negative one. The latent heat flux seasonal cycle is largely tied to the winds. In the AS, the effect of oceanic processes is also strongly tied to the wind with the largest cooling by the upwelling happening during the monsoon when the Findlater jet is strongest. The absence of upwelling is the primary cause for higher SST in the BoB and eastern AS than in the western AS during summer. During winter, the salinity stratification plays a clear role in maintaining a high SST in the BoB and eastern AS. The presence of fresh water near the surface allows the storage of heat below the surface that can later be recovered by entrainment during winter (with a winter contribution of 0.4°C in the eastern AS and 2.1°C in the BoB).

At the interannual timescale, the eastern AS and BoB are strongly controlled by the winds through the latent heat flux anomalies which dominate the net heat flux anomalies. In the western AS, the interannual heat budget is dominated by processes associated to the upwelling regions and most terms in the SST equation do contribute (with the heat forcing and vertical processes being the main ones). The control of the interannual anomalies of SST by the wind is more difficult to establish in this region.

Two potential problems of the model have been aroused during this work. First, the model exhibits a 15 m deep MLD bias in regions of negative Ekman pumping, during winter monsoon in western AS (Figure 3a, upper panel). Secondly, the net heat flux we use in the model appears to be too small compared to recent climatologies such as Southampton Oceanographic Center (SOC) climatology. It is however in reasonnable agreement with NCEP or ECMWF net heat flux in the region. We should note that accurate estimation of heat flux forcings in the tropical Indian Ocean is an important issue that needs further studies as we want to achieve some detailed investigation of SST variability in the region (e.g., MB99, Schott and McCreary, 2001).

In the NIO the interannual variability of SST is weak but can have important climatic impacts as it occurs around high SST of about 28°C. Our analyses suggest that the wind variability plays a strong role in driving the eastern AS and BoB through its impact on latent heat fluxes. It must be reminded, though, that our model does not include interannual variability of the cloud cover and surface air humidity. In the western AS, the mechanisms that drive that variability cannot be reduced to the winds (for example in

1996). Air temperature and relative humidity may also play a role in interannual variability. When SST is lower than air temperature (as in upwelling areas), variations in relative air humidity can result in high variations in latent heat flux, and relative air humidity might become an important parameter. Interannual cloud cover could also be a solution to improve the model interannual simulation which shows some limits in the present configuration. MB99 found a significant contribution from cloud cover and solar radiation in SST anomalies in the northern Indian Ocean. However, sensitivity experiments have been performed with our model on a 2°x2° horizontal resolution grid and showed a weak impact of cloud cover and air humidity interannual variability (differences are about 0.1°C or less on basin scale between the two experiments, not shown). In depth work on careful specification of the surface boundary layer conditions is thus needed to better evaluate the impact of various atmospheric factors on the upper layer heat budget. A coupled model with a correct SST variability could also be a solution to further understand the processes that regulate SST in the northern Indian Ocean.

The penetrative solar heating has been shown to be important. Even if we do not know the part of it which remains in the deeper ocean, it can participate in the transfer of heat to deeper layers as was suggested in Shetye (1986). In this study, we have a high penetrative solar radiation flux due to the thin mixed layer in the NIO. This may partly explain how the NIO manage to regulate its SST by warming the layer beneath the surface. This warming is indeed around 26 W m^{-2} on annual average in the NIO. In the BoB, it results in a negative heat loss of about 10 W m^{-2} which is partly couter balanced by vertical processes warming in winter. However, the penetrative solar radiation depends on the water turbidity and especially on the chlorophyll concentration. In the AS, effects of biological activity on SST have been shown in several studies (Sathyendranath et al., 1991; Nakamoto et al., 2000). Further experiments including some bio-optical parameterizations may be very usefull to assess the role of penetrative solar heat flux on the SST regulation and the suitability of a type I water in the NIO. For example it could give some biological explanation about the 1996 cooling phase. The latter occurs in the late summer monsoon phase when biological activity has been shown to have the most important impact on SST (Sathyendranath et al., 1991).

When plotting raw timeseries of our interannual diagnostics, a great variability is found on intraseasonal timescales. It is taken into account but we did not investigate it. Its potential impact on seasonal and interannual variability through scale interactions has been shown in previous studies (e.g., Goswami and Mohan, 2001) and could also be examined with our model in a future work.

Acknowledgments.

The authors would like to thank the ESOPA team for their work in developping and maintaining the ocean model. All the computations were performed on the NEC SX-5 of the Institut du Développement et des Ressources en Informatique Scientifique (IDRIS), Orsay, France. We thank P. Terray for fruitful discussions about this work. The authors

are thankful to Fabiano Busdraghi for his valuable participation to add the last ARGO floats in the mixed layer depth database. We also thank the two anonymous reviewers for their constructive comments in the revision of the manuscript. Sebastien Masson provided the SAXO plotting environnment based on IDL. This work is supported by a DGA grant (DGA-CNRS 2001-292) and by fundings of the Programme National d'Etude de la Dynamique et du Climat (PNEDC). SSCS and DS thank Departments of Science and Technology and Ocean Development, Govt. of India for financial support. The Institut de Recherche pour le Développement (IRD) provided funding for 3 month visit to the National Institute of Oceanography (NIO), Goa, India, where this work was initiated under Indo-French Program of REsearch in Weather And Climate (IFPREWAC). NIO contribution is 4110.

References

Anderson, S. P., R. A. Weller, and R. B. Lukas, 1996: Surface buoyancy forcing and the mixed layer of the western Pacific warm pool: Observations and 1D model results. *J. Climate*, **9**, 3056-3085.

Behera, S.K., S. Krishnan, and T. Yamagata, 1999: Unusual ocean-atmosphere conditions in the tropical Indian Ocean during 1994. *Geophys. Res. Lett.*, **26**, 3001-3004.

Berliand, M. E., and T. G. Strokina, 1980: Global distribution of the total amount of clouds. Hydrometeorological Publishing House, Leningrad, Russia, 71 pp.

Blanke, B., and P. Delecluse, 1993: Variability of the tropical Atlantic ocean simulated by a general circulation model with two different mixed-layer physics. *J. Phys. Oceanogr.*, **23**, 1363-1388.

Cayan, D. R., 1992: Variability of latent and sensible heat fluxes estimated using bulk formulae. *Atmos.-Ocean*, **30**, 1-42.

Chen, D., A. J. Busalacchi, and L. M. Rothstein, 1994: The roles of vertical mixing, solar radiation and wind stress in a model simulation of the sea surface temperature seasonal cycle in the tropical Pacific ocean. *J. Geophys. Res.*, **99**, 20,345-20,359.

de Boyer Montégut, C., G. Madec, A. S. Fischer, A. Lazar, and D. Iudicone, 2004: Mixed layer depth over the global ocean: An examination of profile data and a profile-based climatology. *J. Geophys. Res.*, **109**, C12003, doi:10.1029/2004JC002378.

Düing, W., and A. Leetmaa, 1980: Arabian Sea cooling: A preliminary heat budget. *J. Phys. Oceanogr.*, **10**, 307-312.

Durand F., S. R. Shetye, J. Vialard, D. Shankar, S. S. C. Shenoi, C. Ethe, and G. Madec, 2004: Impact of temperature inversions on SST evolution in the South-Eastern Arabian Sea during the pre-summer monsoon season. *Geophys. Res. Lett.*, **31**, L01305, doi:10.1029/2003GL018906.

Durand F., D. Shankar, C. de Boyer Montégut, S. S. C. Shenoi, B. Blanke, and G. Madec, 2006: Modeling the salinity effects in the South-Eastern Arabian Sea. *J. Climate*, this issue.

Eigenheer, A., and D. Quadfasel, 2000: Seasonal variability of the Bay of Bengal circulation inferred from TOPEX/Poseidon altimetry. *J. Geophys. Res.*, **105**, 3243-3252.

Findlater, J., 1969: A major low level air current over the Indian Ocean during the northern summer. *Q. J. R. Meteorol. Soc.*, **95**, 280-362.

Fischer, A. S., R. A. Weller, D. L. Rudnick, C. C. Eriksen, C. M. Lee, K. H. Brink, C. A. Fox, and R. R. Leben, 2002: Mesoscale eddies, coastal upwelling, and the upper-ocean heat budget in the Arabian Sea. *Deep-Sea Res. II*, **49**, 2231-2264.

Fischer, A. S., 2000: The upper ocean response to the monsoon in the Arabian Sea. Ph.D. thesis, Mass. Inst. of Technol./Woods Hole Oceanogr. Inst., Woods Hole, Mass.

Gent, P. R., and J. C. McWilliams, 1990: Isopycnal mixing in ocean circulation models. *J. Phys. Oceanogr.*, **20**, 150-155.

Goswami, B. N., and R. S. Ajaya Mohan, 2001: Intraseasonal oscillations and interannual variability of the Indian summer monsoon. *J. Climate*, **14**, 1180-1198.

Halpert, M. S., and G. D. Bell, 1997: Climate assessment for 1996. *Bull. Am. Meteorol. Soc.*, **78**, 1038-1038.

Han, W., J. P. McCreary Jr., and K. E. Kohler, 2001: Influence of precipitation minus evaporation and Bay of Bengal rivers on dynamics, thermodynamics, and mixed layer physics in the upper Indian Ocean. *J. Geophys. Res.*, **106**, 6895-6916.

Jacket, D. R., and T. J. McDougall, 1995: Minimal adjustment of hydrographic data to achieve static stability. *J. Atmos. Oceanic Technol.*, **12**, 381-389.

Jerlov, N. G., 1968: *Optical Oceanography*, 194 pp., Elsevier Sci., Amsterdam.

Kalnay, E., et al., 1996: The NCEP/NCAR 40-Year Reanalysis Project. *Bull. Am. Meteorol. Soc.*, **77**, 437-471.

Konda, M., N. Imasato, and A. Shibata, 2002: Interannual variability of the sea-surface temperature in the Indian Ocean in response to the air-sea turbulent heat exchange. *Deep-Sea Res. II*, **49**, 1527-2548.

Lander, M. A., E. J. Trehubenko, and C. P. Guard, 1999: Eastern hemisphere tropical cyclones of 1996. *Mon. Weather Rev.*, **127**, 1274-1300.

Lee, C. M., B. H. Jones, K. H. Brink, and A. S. Fischer, 2000: The upper-ocean response to monsoonal forcing in the Arabian Sea: seasonal and spatial variability. *Deep-Sea Res. II*, **47**, 1177-1226.

Levitus, S., 1998: Climatological Atlas of the world ocean. *Tech. Rep. 13*, NOAA, Rockville, Md.

Lewis, M. R., M.-E. Carr, G. C. Feldman, W. Esaias, and C. McClain, 1990: Influence of penetrating solar radiation on the heat budget of the equatorial Pacific Ocean. *Nature*, **347**, 543-545.

Li, T., Y. Zhang, C.-P. Chang, and B. Wang, 2001: On the relationship between indian ocean seas surface temperature and asian summer monsoon. *Geophys. Res. Lett.*, **28**, 2843-2846.

Madec, G., and M. Imbard, 1996: A global ocean mesh to overcome the North Pole singularity. *Clim. Dyn.*, **12**, 381-388.

Madec, G., P. Delecluse, M. Imbard, and C. Levy, 1999: OPA 8.1 Ocean General Circulation Model reference manual. *Notes du pôle de modélisation*, Institut Pierre Simon Laplace (IPSL), France, n°XX, 91 pp.

Masson, S., et al., 2005: Impact of barrier layer on winter-spring variability of the South-Eastern Arabian Sea. *Geophys. Res. Lett.*, **32**, L07703,doi:10.1029/2004GL021980.

McCreary, J. P., and P. K. Kundu, 1989: A numerical investigation of sea surface temperature variability in the Arabian Sea. *J. Geophys. Res.*, **94**, 16097-16114.

McCreary, J. P., P. K. Kundu, and R. L. Molinari, 1993: A numerical investigation of dynamics, thermodynamics and mixed-layer processes in the Indian Ocean. *Progress in Oceanography*, **31**, 181-244.

McCreary, J. P., Jr., K. E. Kohler, R. R. Hood, S. Smith, J. Kindle, A. S. Fischer, and R. A. Weller, 2001: Influences of diurnal and intraseasonal forcing on mixed-layer and biological variability in the central Arabian Sea. *J. Geophys. Res.*, **106**, 7139-7156.

Merryfield, W. J., G. Holloway, and A. E. Gargett, 1999: A global ocean model with double diffusive mixing. *J. Phys. Oceanogr.*, **29**, 1124-1142.

Mignot, J., C. de Boyer Montégut, A. Lazar, and S. Cravatte, 2006: Control of salinity on the mixed layer depth in the world ocean. submitted to *J. Geophys. Res.*

Molinari, R. L., J. Swallow, and J. F. Festa, 1986: Evolution of the near-surface thermal structure in the western Indian Ocean during FGGE, 1979. *J. Mar. Res.*, **44**, 739-762.

Murray, R. J., 1996: Explicit generation of orthogonal grids for ocean models. *J. Comput. Phys.*, **126**, 251-273.

Murtugudde, R., and A. J. Busalacchi, 1999: Interannual variability of the dynamics and thermodynamics of the tropical Indian Ocean. *J. Climate*, **12**, 2300-2326.

Nakamoto, S., S. Prasanna Kumar, J. M. Oberhuber, K. Muneyama, and R. Frouin, 2000: Chlorophyll modulation of sea surface temperature in the Arabian Sea in a mixed layer isopycnal general circulation model. *Geophys. Res. Lett.*, **27**, 747-750.

Prasad, T. G., 2004: A comparison of mixed-layer dynamics between the Arabian Sea and Bay of Bengal: One-dimensional model results. *J. Geophys. Res.*, **109**, C03035, doi:10.1029/2003JC002000.

Qiu, B., S. Chen, and P. Hacker, 2004: Synoptic-scale air-sea flux forcing in the western north Pacific: observations and their impact on SST and the mixed layer. *J. Phys. Oceanogr.*, **34**, 2148-2159.

Rao, R. R., K.V.S. Ramam, D.S. Rao, and M.X. Joseph, 1985: Surface heat budget estimates at selected regions of the north Indian Ocean during Monsoon-77. *Mausam*, **36**, 21-32.

Rao, R. R., R. L. Molinari, and J. F. Festa, 1989: Evolution of the climatological near-surface thermal structure of the tropical indian ocean. 1. Description of mean monthly mixed layer depth, and sea surface temperature, surface current, and surface meteorological fields. *J. Geophys. Res.*, **94**, 10,801-10,815.

Rao, R. R., and R. Sivakumar, 2000: Seasonal variability of near-surface thermal structure and heat budget of the mixed layer of the Tropical Indian Ocean from a new global ocean temperature climatology. *J. Geophys. Res.*, **105**, 995-1015.

Rao, R. R., and R. Sivakumar, 2003: Seasonal variability of sea surface salinity and salt budget of the mixed layer of the north indian ocean. *J. Geophys. Res.*, **108**, 3009, doi:10.1029/2001JC000907.

Reynolds, R. W., and T. M. Smith, 1994: Improved global sea surface temperature analysis using optimum interpolation. *J. Climate*, **7**, 929-948.

Rochford, P. A., J. C. Kindle, P. C. Gallacher, and R. A. Weller, 2000: Sensitivity of the Arabian Sea mixed layer to 1994-1995 operational wind products. *J. Geophys. Res.*, **105**, 14,141-14,162.

Roullet, G., and G. Madec, 2000: Salt conservation, free surface and varying volume: a new formulation for Ocean GCMs. *J. Geophys. Res.*, **105**, 23,927-23,942.

Saji, N. H., B. N. Goswami, P. N. Vinayachandran, and T. Yamagata, 1999: A dipole mode in the tropical Indian Ocean. *Nature*, **401**, 360-363.

Sathyendranath, S., A. D. Gouveia, S. R. Shetye, P. Ravindran, and T. Platt, 1991: Biological control of surface temperature in the Arabian Sea. *Nature*, **349**, 54-56.

Schott, F. A., and J. P. McCreary, 2001: The monsoon circulation of the Indian Ocean. *Progress in Oceanography*, **51**, 1-123.

Sengupta, D., P. K. Ray, and G. S. Bhat, 2002: Spring warming of the eastern Arabian Sea and Bay of Bengal from buoy data. *Geophys. Res. Lett.*, **29**, 1734, doi:10.1029/2002GL015340.

Shankar, D., V.V. Gopalakrishna, S.S.C. Shenoi, F.Durand, S.R. Shetye, C.K. Rajan, Z. Johnson, N. Araligidad, and G.S. Michael, 2004: Observational evidence for westward propagation of temperature inversions in the southeastern Arabian Sea. *Geophys. Res. Lett.*, **31**, doi:10.1029/2004GL019652.

Shankar, D., P.N. Vinayachandran, and A.S. Unnikrishnan, 2002: The monsoon currents in the north Indian Ocean. *Progress in Oceanography*, **52**, 63-120.

Shenoi, S. S. C., D. Shankar, and S. R. Shetye, 2002: Differences in heat budgets of the near-surface Arabian Sea and Bay of Bengal: Implications for the summer monsoon. *J. Geophys. Res.*, **107**, 10.1029/2000JC000679.

Shenoi, S. S. C., D. Shankar, and S. R. Shetye, 2004: Remote forcing annihilates barrier layer in southeastern Arabian Sea. *Geophys. Res. Lett.*, **31**, L05307, doi:10.1029/2003GL019270.

Shenoi, S. S. C., D. Shankar, and S. R. Shetye, 2005a: On the accuracy of the Simple Ocean Data Analysis for estimating heat budgets of the near-surface Arabian Sea and Bay of Bengal. *J. Phys. Oceanog.*, **35**, 395-400.

Shenoi, S.S.C., D. Shankar, V.V. Gopalakrishna, and F. Durand, 2005b. Role of ocean in the genesis and annihilation of the core of the warm pool in the southeastern Arabian Sea. *Mausam*, **56**, 147-160.

Shetye, S. R., 1986: A model study of the seasonal cycle of the Arabian Sea surface temperature. *J. Mar. Res.*, **44**, 521-542.

Shetye, S. R., S. S. C. Shenoi, A. D. Gouveia, G. S. Michael, D. Sundar, and G. Nampoothiri, 1991: Wind-driven coastal upwelling along the western boundary of the Bay of Bangal during the southwest monsoon. *Cont. Shelf Res.*, **11**, 1397-1408, 1991.

Smith, W. H. F., and D. T. Sandwell, 1997: Global sea floor topography from satellite altimetry and ship depth soundings. *Science*, **277**, 1956-1962.

Timmermann, R., H. Goosse, G. Madec, T. Fichefet, C. Ethe, and V. Dulière, 2005: On the representation of high latitude processes in the ORCA-LIM global coupled sea ice-ocean model. *Ocean Modelling*, **8**, 175-201.

Trenberth, K. E., J. G. Olson, and W. G. Large, 1989: A global ocean wind stress climatology based on the ECMWF analyses. National Center for Atmospheric Research, NCAR/TN-338+STR, Boulder, Colorado, 93 pp.

UNESCO (Ed.), 1996: Discharge of selected rivers of the world. Volume II (Part II), UNESCO Publishing.

Vecchi, G. A., and D. E. Harrison, 2002: Monsoon Breaks and Subseasonal Sea Surface Temperature Variability in the Bay of Bengal. *J. Climate*, **15**, 1485-1493.

Vecchi, G. A., S.-P. Xie, and A. S. Fischer, 2004: Ocean-Atmosphere Covariability in the Western Arabian Sea. *J. Climate*, **17**, 1213-1224.

Vialard, J., and P. Delecluse, 1998: An OGCM study for the TOGA decade. Part I: Role of salinity in the physics of the Western Pacific fresh pool. *J. Phys. Oceanog.*, **28**, 1071-1088.

Vialard, J., C. Menkes, J.-P. Boulanger, P. Delecluse, E. Guilyardi, M. J. McPhaden, and G. Madec, 2001: A model study of oceanic mechanisms affecting equatorial pacific sea surface temperature during the 1997-98 El Niño. *J. Phys. Oceanog.*, **31**, 1649-1675.

Vinayachandran, P. N., and T. Yamagata, 1998: Monsoon response of the sea around Sri Lanka: Generation of thermal domes and anticyclonic vortices. *J. Phys. Oceanog.*, **28**, 1946-1960.

Vinayachandran, P. N., V. S. N. Murty, and V. Ramesh Babu, 2002: Observations of barrier layer formation in the Bay of Bengal during summer monsoon. *J. Geophys. Res.*, **107**, 8018, doi:1029/2001JC000831.

Vinayachandran, P. N., 2004: Summer cooling of the Arabian Sea during contrasting monsoons. *Geophys. Res. Lett.*, **31**, L13306, doi:10.1029/2004GL019961.

Webster, P. J., V. O. Magaña, T. N. Palmer, J. Shukla, R. A. Tomas, M. Yanai, and T. Yasunari, 1998: Monsoons: Processes, predictability, and the prospects for prediction. *J. Geophys. Res.*, **103**, 14,451-14,510.

Webster, P. J., A. M. Moore, J. P. Loschnigg, and R. R. Leben, 1999: Coupled ocean-atmosphere dynamics in the Indian Ocean during 1997-98. *Nature*, **40**, 356-360.

Weller, R. A., M. F. Baumgartner, S. A. Josey, A. S. Fischer, and J. C. Kindle, 1998: Atmospheric forcing in the Arabian Sea during 1994-1995: observations and comparisons with climatology and models. *Deep-Sea Res. II*, **45**, 1961-1999.

Xie, P., and P. A. Arkin, 1996: Analysis of global monthly precipitation using gauge observations, satellite estimates and numerical model predictions. *J. Climate*, **9**, 840-858.

Yu, Z., and J. P. McCreary Jr., 2004: Assessing precipitation products in the Indian Ocean using an ocean model. *J. Geophys. Res.*, **109**, C05013, doi:10.1029/2003JC002106.

Yu, L., and M. M. Rienecker, 2000: Indian Ocean warming of 1997-1998. *J. Geophys. Res.*, **105**, 16,923-16,939.

FIGURE CAPTIONS LIST :

Figure 1 : Map of the Northern Indian Ocean (NIO) along with the main rivers of the region. River runoffs parameterized in the model are shown with dots whose size increases with increasing mean annual discharge of the river. The NIO is divided by the indian subcontinent into two semienclosed basins, the Arabian Sea (AS) and the Bay of Bengal (BoB). The dashed meridional line located at 65°E separates between the western AS and the eastern AS. The grey area corresponds to the western AS coastal zone (about 350 km away from the coast). The 6°N parallel indicates the southern limit of the basins considered in this study.

Figure 2 : Seasonal maps of Mixed Layer Depth (MLD) for December-January-February (DJF), March-April-May (MAM), June-July-August (JJA) and September-October-November (SON). (a) MLD from the model, defined as the depth at which density is 0.01 kg m^{-3} greater than the sea surface density. (b) MLD from de Boyer Montégut et al. (2004), defined with a $\Delta\sigma_\theta = 0.03$ kg m^{-3} from the density at 10 m depth. Further comments are given in the text about the criterion difference between the data and the model. The seasonal climatology for the model is computed over 1993-2000. The black arrow in DJF and JJA seasons panels indicates the climatological axis of the winds, especially the Findlater (1969) Jet in JJA. Symbols also denotes positive ($\odot$) or negative ($\otimes$) Ekman pumping on each side of the winds axis. Contour interval is 5 m from 10 to 40 m, and 10 m from 40 m to higher values.

Figure 3 : Mixed layer depth (MLD), mixed layer temperature (T[ml], a proxy for SST), temperature integrated over 0-50 m (T50) and barrier layer thickness (BLT) computed following de Boyer Montégut et al. (2004) (upper panel), SST seasonal tendencies in the mixed layer (middle panel), and surface heat fluxes (positive into the ocean), effective net heat flux in the mixed layer (Qeff=Qnet-Qpen), net shortwave radiation flux in the mixed layer (Qsw[ml]), net shortwave radiation flux at the surface (Qsw), latent heat flux (Qlat), net longwave radiation flux (Qlw), sensible heat flux (Qsens) and penetrative solar heat flux (Qpen=Qsw-Qsw[ml]) (lower panel), in (a) Western Arabian Sea, (b) Eastern Arabian Sea, and (c) Bay of Bengal.

Figure 4 : SST seasonal tendencies in the mixed layer for (a) western Arabian Sea coastal zone (grey area in Figure 1), and (b) the rest of western Arabian Sea (central western Arabian Sea). Note that the range in tendency is greater than the one used in Figure 3.

Figure 5 : Map of climatological heating tendency rate computed over 1993-2000 for subsurface vertical processes in winter (December-January-February). Contours are indicated from -0.6 to 0.6 °C/month with a contour interval of 0.2 °C/month. Positive values, indicating warming by the subsurface, are shaded with a greyscale every 0.2 °C/month.

Figure 6 : SST interannual anomaly with respect to the 1993-2000 seasonal cycle in (a) Western Arabian Sea, (b) Eastern Arabian Sea, and (c) Bay of Bengal. Data are filtered with a 90-days running mean filter to remove any subseasonal high frequency variability. December-January-February and June-July-August periods have been shaded to indicate respectively the winter and summer monsoons.

Figure 7 : Interannual anomalies of model mixed layer depth (MLD) and wind speed from ERS data (upper panel), interannual anomalies of SST tendencies (middle panel), and interannual anomalies of net downward heat flux (Qnet), downward latent heat flux computed with model SST (Qlat), downward latent heat flux computed with Reynolds SST (Qlat[Reynolds]), downward latent heat flux computed with Reynolds SST and climatological value of air-sea humidity gradient (Qlat[Reynolds/Winds]) (lower panel) in the Western Arabian Sea. Anomalies are computed with respect to the 1993-2000 seasonal cycle. Data are filtered with a 90-days running mean filter to remove any subseasonal high frequency variability. December-January-February and June-July-August periods have been shaded to indicate respectively the winter and summer monsoons.

Figure 8 : Same as Figure 7 for the Eastern Arabian Sea.

Figure 9 : Same as Figure 7 for the Bay of Bengal.

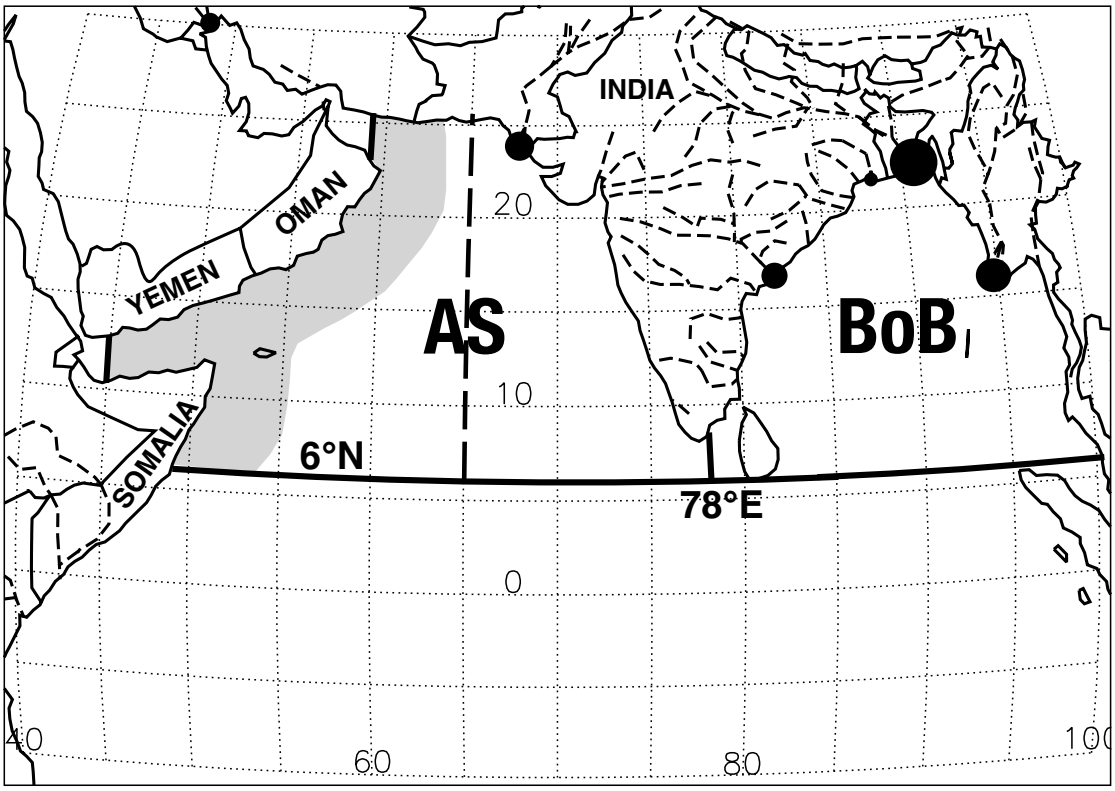

Figure 1: Map of the Northern Indian Ocean (NIO) along with the main rivers of the region. River runoffs parameterized in the model are shown with dots whose size increases with increasing mean annual discharge of the river. The NIO is divided by the indian subcontinent into two semienclosed basins, the Arabian Sea (AS) and the Bay of Bengal (BoB). The dashed meridional line located at 65°E separates between the western AS and the eastern AS. The grey area corresponds to the western AS coastal zone (about 350 km away from the coast). The 6°N parallel indicates the southern limit of the basins considered in this study.

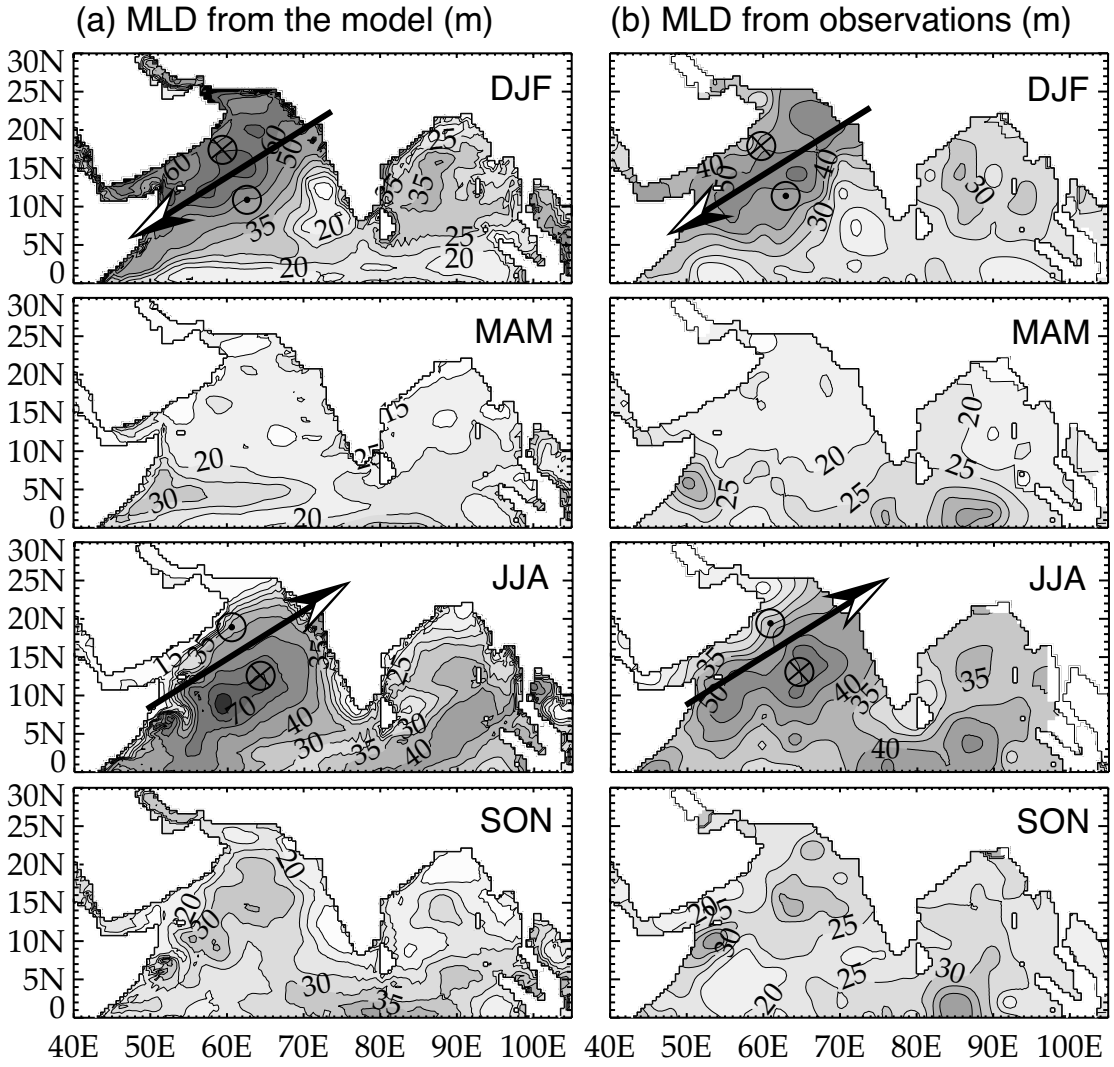

Figure 2: Seasonal maps of Mixed Layer Depth (MLD) for December-January-February (DJF), March-April-May (MAM), June-July-August (JJA) and September-October-November (SON). (a) MLD from the model, defined as the depth at which density is 0.01 kg m^{-3} greater than the sea surface density. (b) MLD from de Boyer Montégut et al. (2004), defined with a $\Delta\sigma_\theta = 0.03$ kg m^{-3} from the density at 10 m depth. Further comments are given in the text about the criterion difference between the data and the model. The seasonal climatology for the model is computed over 1993-2000. The black arrow in DJF and JJA seasons panels indicates the climatological axis of the winds, especially the Findlater (1969) Jet in JJA. Symbols also denotes positive ($\odot$) or negative ($\otimes$) Ekman pumping on each side of the winds axis. Contour interval is 5 m from 10 to 40 m, and 10 m from 40 m to higher values.

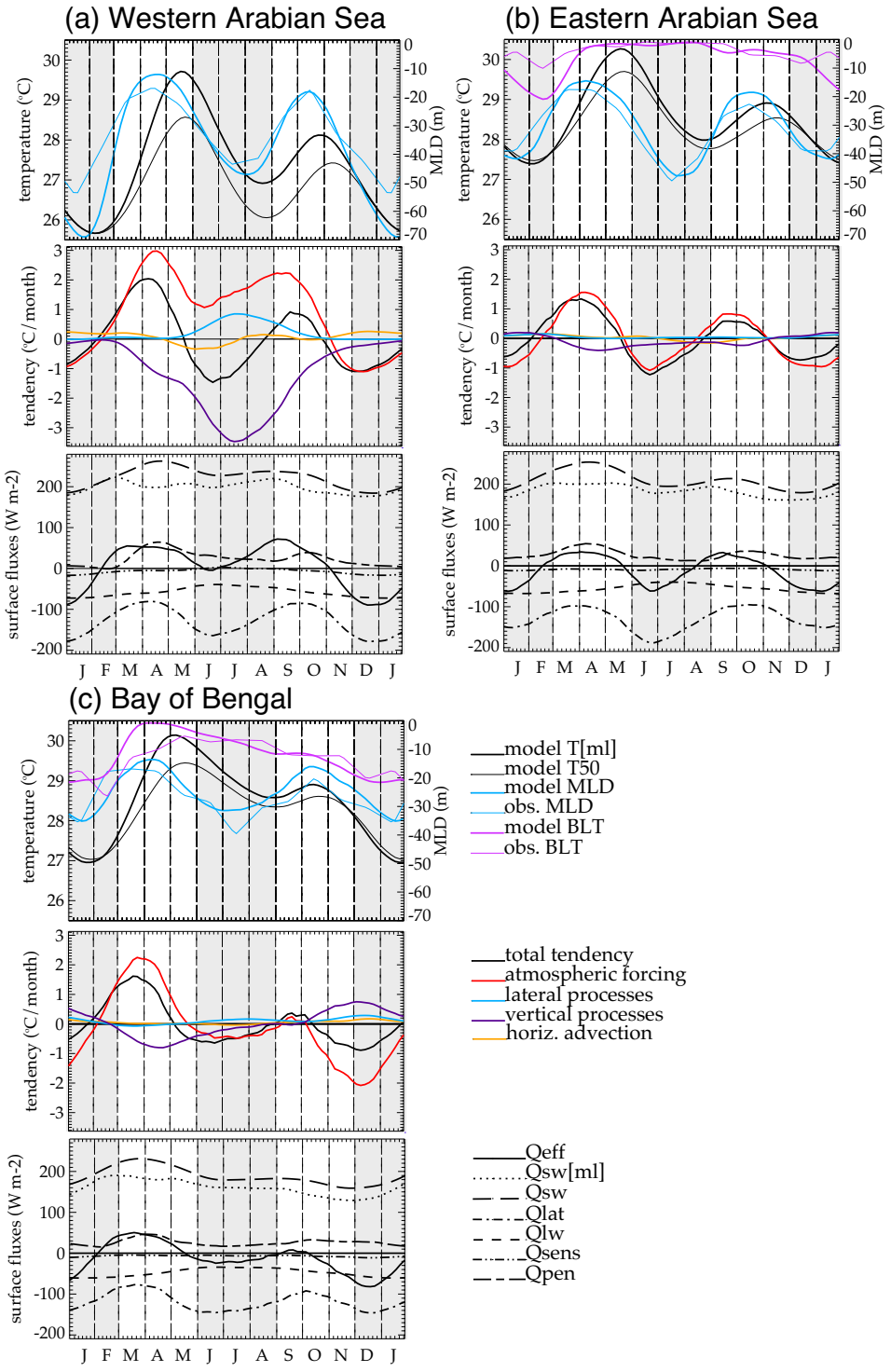

Figure 3: Mixed layer depth (MLD), mixed layer temperature (T[ml], a proxy for SST), temperature integrated over 0-50 m (T50) and barrier layer thickness (BLT) computed following de Boyer Montégut et al. (2004) (upper panel), SST seasonal tendencies in the mixed layer (middle panel), and surface heat fluxes (positive into the ocean), effective net heat flux in the mixed layer (Qeff=Qnet-Qpen), net shortwave radiation flux in the mixed layer (Qsw[ml]), net shortwave radiation flux at the surface (Qsw), latent heat flux (Qlat), net longwave radiation flux (Qlw), sensible heat flux (Qsens) and penetrative solar heat flux (Qpen=Qsw-Qsw[ml]) (lower panel), in (a) Western Arabian Sea, (b) Eastern Arabian Sea, and (c) Bay of Bengal.

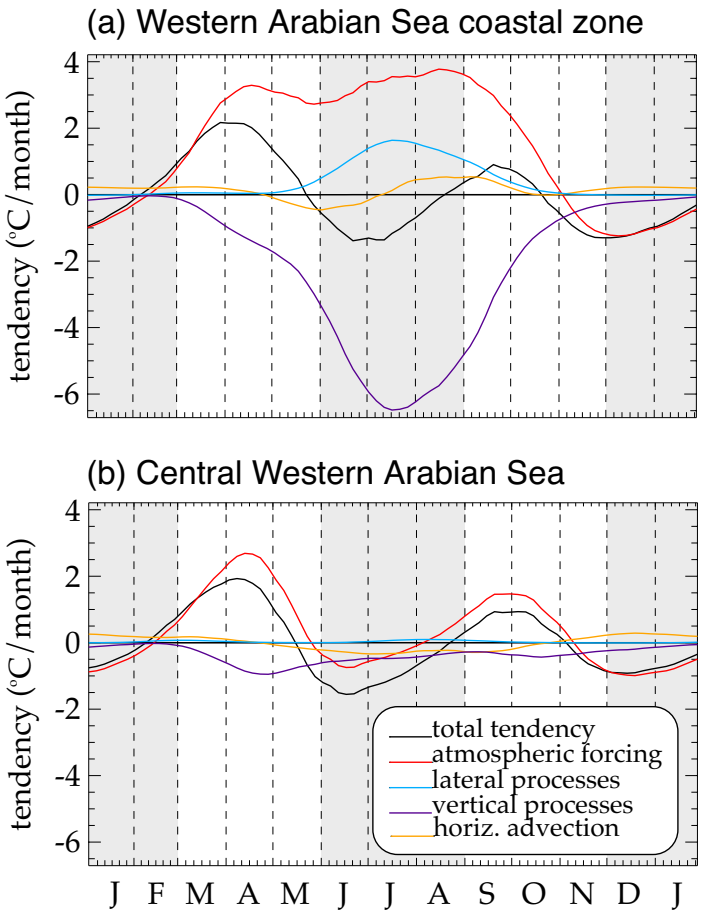

Figure 4: SST seasonal tendencies in the mixed layer for (a) western Arabian Sea coastal zone (grey area in Figure 1), and (b) the rest of western Arabian Sea (central western Arabian Sea). Note that the range in tendency is greater than the one used in Figure 3.

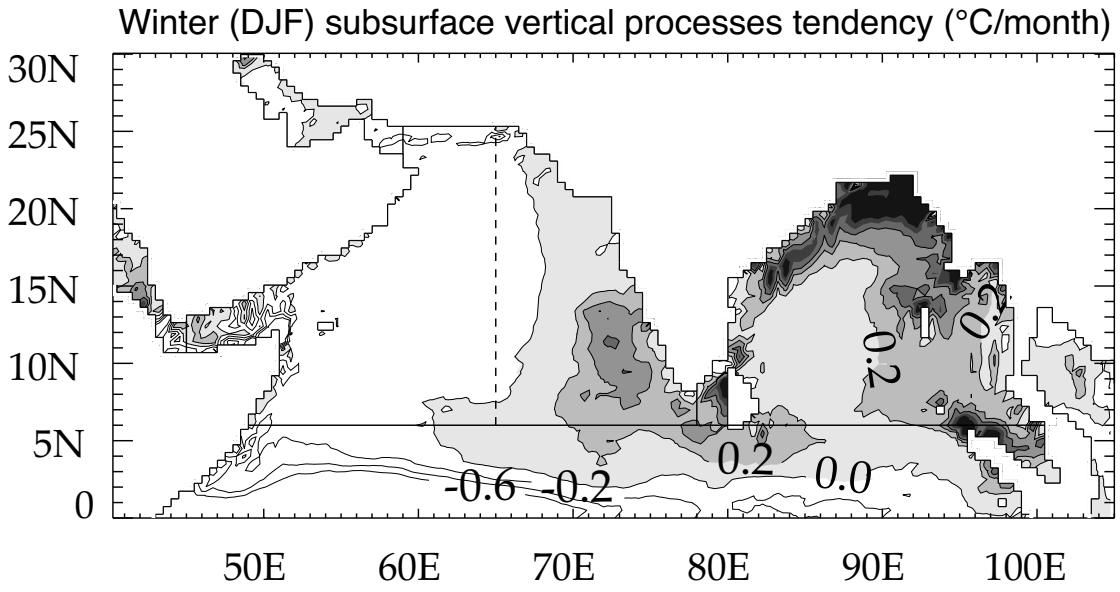

Figure 5: Map of climatological heating tendency rate computed over 1993-2000 for subsurface vertical processes in winter (December-January-February). Contours are indicated from -0.6 to 0.6 °C/month with a contour interval of 0.2 °C/month. Positive values, indicating warming by the subsurface, are shaded with a greyscale every 0.2 °C/month.

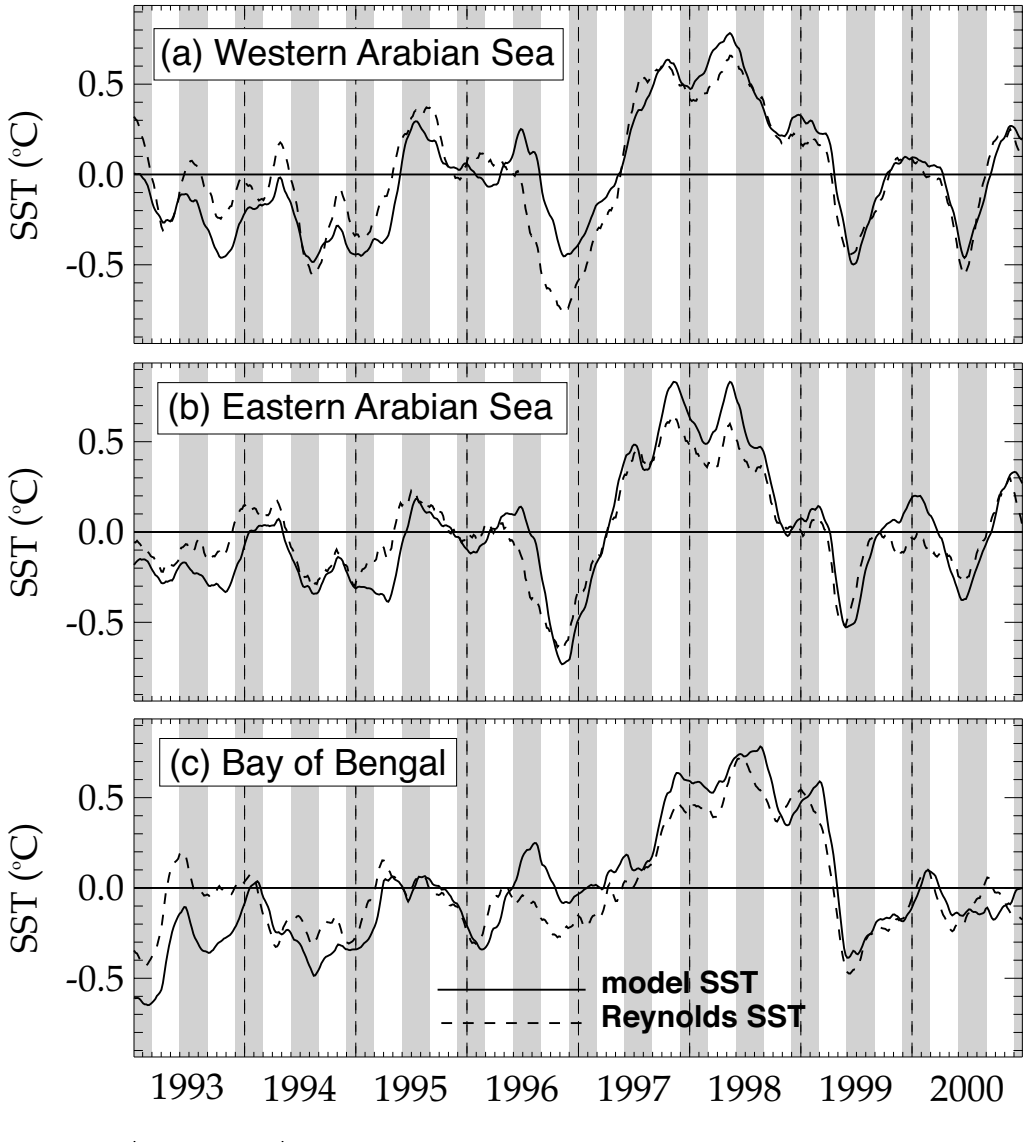

Figure 6: SST interannual anomaly with respect to the 1993-2000 seasonal cycle in (a) Western Arabian Sea, (b) Eastern Arabian Sea, and (c) Bay of Bengal. Data are filtered with a 90-days running mean filter to remove any subseasonal high frequency variability. December-January-February and June-July-August periods have been shaded to indicate respectively the winter and summer monsoons.

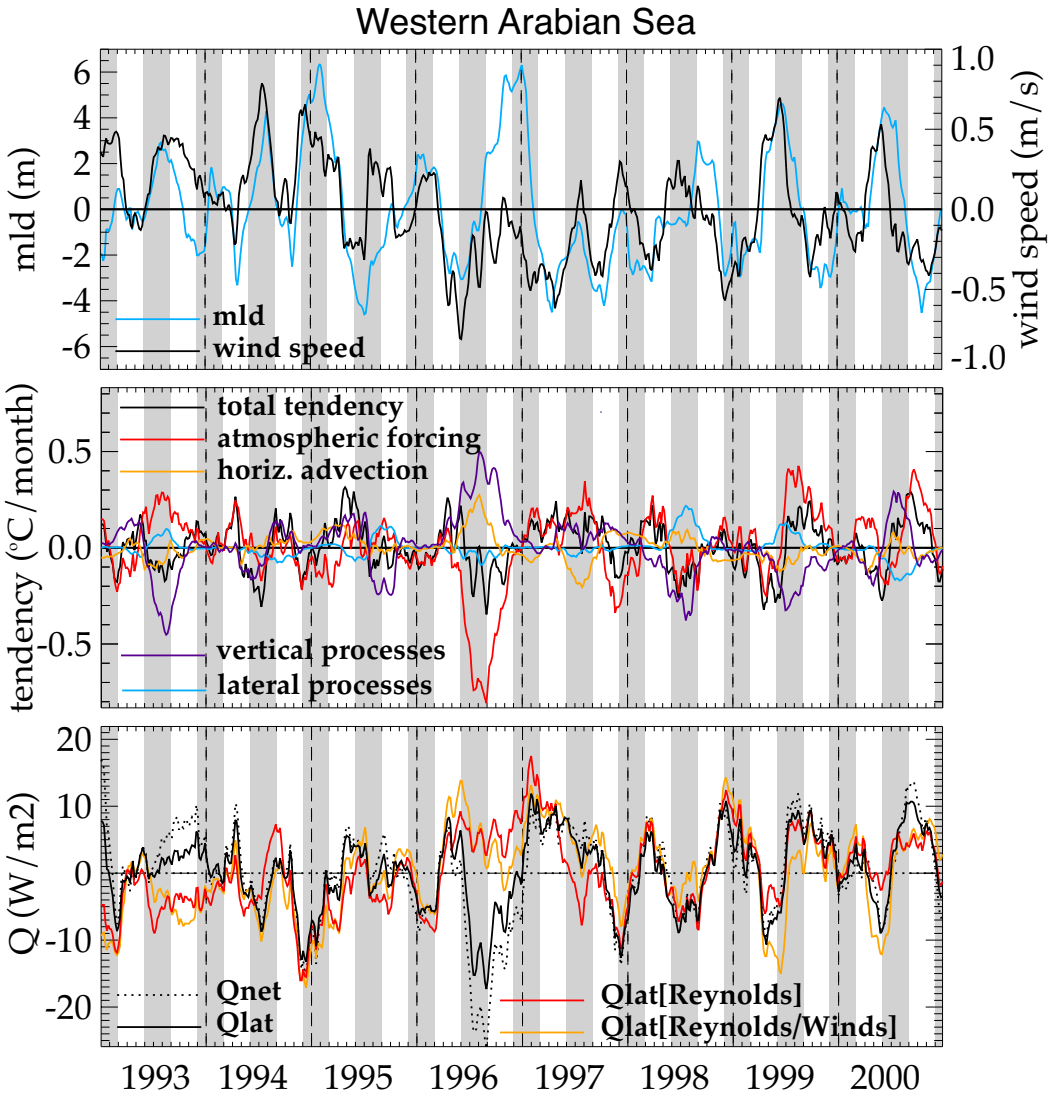

Figure 7: Interannual anomalies of model mixed layer depth (MLD) and wind speed from ERS data (upper panel), interannual anomalies of SST tendencies (middle panel), and interannual anomalies of net downward heat flux (Qnet), downward latent heat flux computed with model SST (Qlat), downward latent heat flux computed with Reynolds SST (Qlat[Reynolds]), downward latent heat flux computed with Reynolds SST and climatological value of air-sea humidity gradient (Qlat[Reynolds/Winds]) (lower panel) in the Western Arabian Sea. Anomalies are computed with respect to the 1993-2000 seasonal cycle. Data are filtered with a 90-days running mean filter to remove any subseasonal high frequency variability. December-January-February and June-July-August periods have been shaded to indicate respectively the winter and summer monsoons.

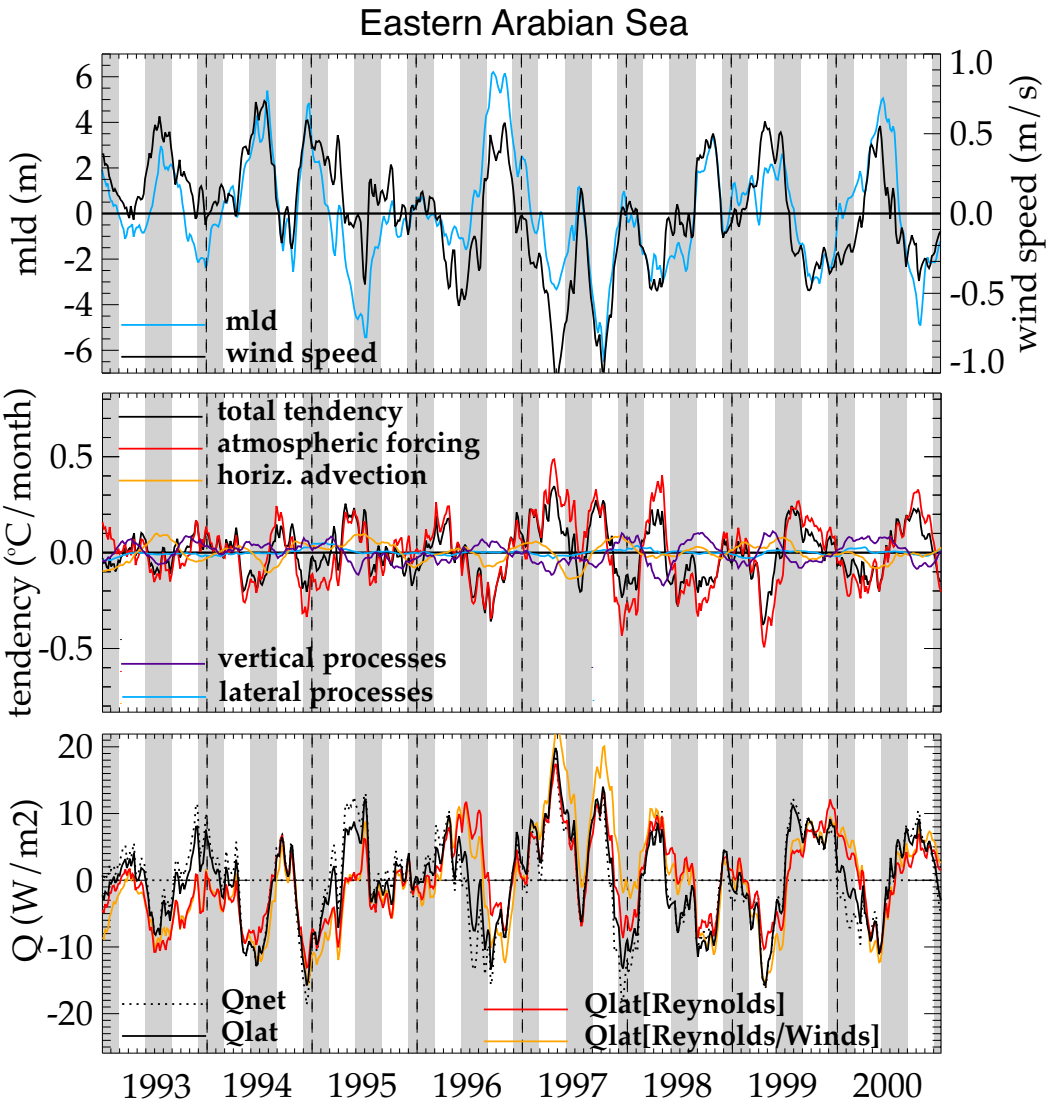

Figure 8: Same as Figure 7 for the Eastern Arabian Sea.

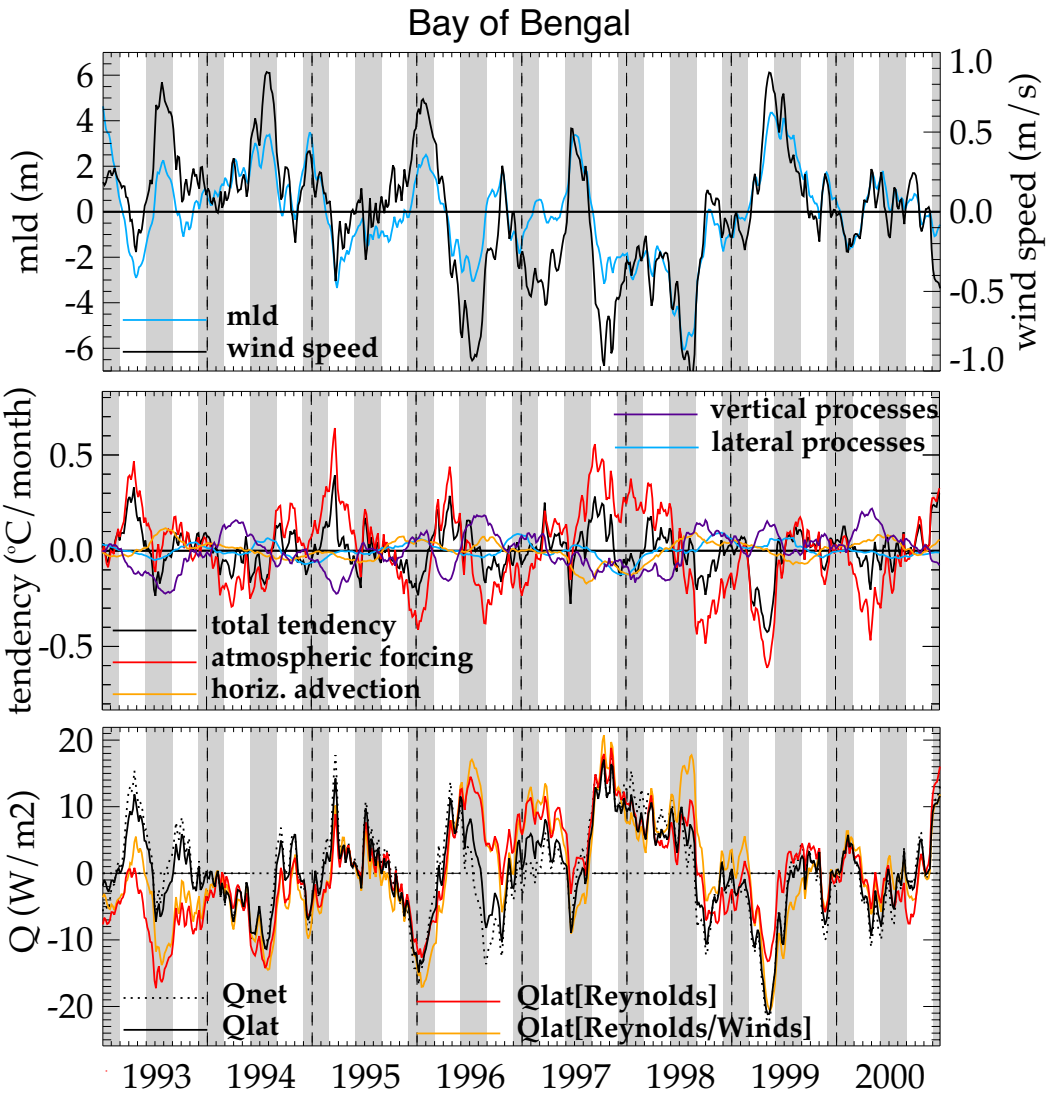

Figure 9: Same as Figure 7 for the Bay of Bengal.

region	Q_{net}	Q_{pen}	Q_{eff}	Q_{sw} std dev	$Q_{sw\ in\ mld}$ std dev
west Arabian Sea	35.7	25.2	10.4	23.0	13.7
east Arabian Sea	17.8	26.9	-9.1	22.7	14.4
Bay of Bengal	17.9	28.3	-10.4	22.0	19.0

Table 1: Annual heat fluxes for the three regions of interest. Q_{net} is the net downward heat flux at the surface, Q_{pen} is the penetrative solar heat flux and Q_{eff} is the effective heat flux available to warm the mixed layer (Q_{eff} =Q_{net}-Q_{pen}). The standard deviation of the solar heat flux (Q_{sw}) and of the solar heat flux into the mixed layer ($Q_{sw\ in\ mld}$) are also shown. Fluxes are in W m^{-2}.

region	T_{fall}	T_{winter}	ΔT	barrier layer warming
west Arabian Sea	28.2	25.7	-2.5	0.0
east Arabian Sea	28.9	27.4	-1.5	0.4
Bay of Bengal	28.9	27.0	-1.9	2.1

Table 2: Influence of salinity stratification on mixed layer heat budget through barrier layer warming effect during the winter monsoon cooling phase in the three regions of interest. Temperatures are in °C.